POLARIZATION AND PHASE CHARACTERIZATION OF SIDE-POLISHED OPTICAL FIBERS

A Thesis Submitted to
the Graduate School of Engineering and Sciences of
İzmir Institute of Technology
in Partial Fulfillment of the Requirements for the Degree of

MASTER OF SCIENCE

in Electronics and Communication Engineering

by
Yunus Emre KARATAŞ

December 2018
İZMİR

We approve the thesis of **Yunus Emre KARATAŞ**

Examining Committee Members:

Prof. Dr. Mehmet Salih DİNLEYİCİ
Department of Electrical and Electronics Engineering
İzmir Institute of Technology

Prof. Dr. Alp KUŞTEPELİ
Department of Electrical and Electronics Engineering
İzmir Institute of Technology

Prof. Dr. Yeşim ZORAL
Department of Electrical and Electronics Engineering
Dokuz Eylül University

5 December 2018

Prof. Dr. Mehmet Salih DİNLEYİCİ
Supervisor, Department of Electrical and Electronics Engineering
İzmir Institute of Technology

Prof. Dr. Enver TATLICIOĞLU
Head of the Department of
Electrical and Electronics Engineering

Prof. Dr. Aysun SOFUOĞLU
Dean of the Graduate School of
Engineering and Sciences

ACKNOWLEDGMENTS

Firstly, I would like to express my sincere gratitude to my advisor Prof. Dr. M. Salih Dinleyici for his patience, motivation, guidance and immense knowledge. He has provided me with continuous support during my thesis stage.

Besides my advisor, I would like to thank the rest of my thesis committee for their insightful comment and encouragements.

I would like to express my genuine thanks to Assist. Prof. Dr. Osman Akın and Çağın Ekici for their valuable supports and favors.

I owe special thanks to my mother Leyla Karataş, my father Asıman Fedai Karataş, my sister Özlem Karataş, my brother Ahmet Karataş and Turgut family for supporting me spiritually through this thesis stage and my life in general.

Last but not least, very special thank to my fiancée Çiğdem Turgut for being with me all the time. She has always been my motivation and encouragement source.

ABSTRACT

POLARIZATION AND PHASE CHARACTERIZATION OF SIDE-POLISHED OPTICAL FIBERS

In this thesis, the polarization and phase properties of the side-polished optical fiber (SPOF) are aimed to characterize. The Linearly Polarized (LP) modes of standard optical fibers have been affected by the side-polished geometry which breaking symmetry. At the side-polished area guided modes couple to non-symmetric modes and phase shift occurs due to the birefringent property of the SPOF. That kind of structure has an excellent usage potential as a portable optical sensor or optical fiber communication device.

It was primarily concentrated on the LP modes of the standard optical fiber. LP mode field solutions extracted from Maxwell Equations were calculated with MATLAB, and mode intensity distributions were constructed accordingly. The calculated intensity distributions were utilized for figuring out the mode content of the outputs of the two-mode experiment. The recorded CCD Camera images were matched with the calculated intensity distributions, and then the best-matched LP mode combination was selected as output mode content.

In the single-mode experiment at the side-polished area, quasi-degenerate fundamental modes occur. According to the state of polarization of the modes, they suffer attenuation and phase shift in different levels. Therefore, after the side-polished area, degenerate fundamental modes propagate together with a particular phase difference. This situation composes elliptical polarization at the output. Various modal polarization rotation and phase shifts were observed, and then polarization ellipses were obtained with MATLAB. The resultant ellipses demonstrate that the effect of SPOF on guided modes varies with the angle of input polarization.

ÖZET

KENARI İNCELTİLMİŞ OPTİK FİBERLERİN POLARİZASYON VE FAZ KARAKTERİZASYONU

Bu tezde, kenarı inceltilmiş optik fiberlerin (SPOF) polarizasyon ve faz özelliklerinin karakterize edilmesi amaçlanmıştır. Standart optik fiberlerin Lineer Polarize (LP) modları, simetriyi bozan kenarı inceltilmiş geometriden etkilenir. Kenarı inceltilmiş bölgede, kılavuzlanan modlar anti-simetrik modlara kuple olurlar ve SPOF'un çift kırınım özelliğine bağlı olarak bunlar arasında faz kayması meydana gelir. Bu tür bir yapı taşınabilir optik sensör veya optik fiber haberleşme cihazı olarak kullanılabilmesi için büyük bir potansiyele sahiptir.

Öncelikle standart bir optik fiberin LP modları üzerine odaklanıldı. Maxwell Denklemlerinden çıkarılan LP mod alan çözümleri MATLAB ile hesaplandı ve mod yoğunluk dağılımları buna göre oluşturuldu. İki-modlu deneyin çıktılarının mod içeriğini belirlemek için hesaplanan yoğunluk dağılımları kullanıldı. Kaydedilen CCD Kamera görüntüleri hesaplanan yoğunluk dağılımları ile eşleştirildi ve daha sonra en iyi eşleşen LP mod kombinasyonu çıkışın mod içeriği olarak seçildi.

Tek-modlu deneyde kenarı inceltilmiş alanda yarı-dejenere temel modlar meydana gelir. Bu modlar polarizasyon durumlarına göre farklı seviyelerde zayıflama ve faz kayması yaşarlar. Bu nedenle, kenarı inceltilmiş alandan sonra, dejenere temel modları belirli bir faz farkı ile birlikte yayılırlar. Bu durum çıkışta eliptik polarizasyon oluşturur. Çeşitli modal polarizasyon rotasyonu ve faz kaymaları gözlenmiştir, ve daha sonra polarizasyon elipsleri MATLAB ile elde edilmiştir. Ortaya çıkan elipsler, kenarı inceltilmiş optik fiberin kılavuzlanan modlar üzerine olan etkisinin giriş polarizasyon açısına bağlı olarak değiştiğini göstermektedir.

TABLE OF CONTENTS

LIST OF FIGURES

Figure **Page**

LIST OF TABLES

LIST OF ABBREVIATIONS

SPOF . . . . . Side-Polished Optical Fiber
SOP . . . . . State of Polarization
CCD . . . . . Charge Coupled Device
SPR . . . . . Surface Plasmon Resonance
TIR . . . . . Total Internal Reflection
LSM . . . . . Least Square Method

CHAPTER 1

INTRODUCTION

From the beginning of early $1980's$ it is common to use polished optical fiber in sensing refractive index [1-7]. When the first idea comes out, the measurements carried out with cladding partially stripped off optical fiber by measuring the output power [1]. Till 1990 polishing and measurements techniques had been improved, then the first fiber optic surface plasmon resonance (SPR) technique was launched out [8], and this invention was the reporter that determination of much smaller refractive index variation will be achieved. Besides this sensing region development, to sense refractive index more precisely, spectroscopic methods have been developed as a measurement technique. However, this technique uses generally bulky and expensive measurement modules. Thus, this prevents the system being portable. To sense refractive index with portable, inexpensive and simple system, there is an alternative method which examines birefringence effect of the side-polished region using a non-spectroscopic technique [9]. In this method, polarization and phase shift properties of a clad free optical fiber are taken into account. Intensities of phase shifted vertical and horizontally polarized fields were measured to sense refractive index of the ambient via balance detector. In the same way, in this thesis polarization and phase properties of the side-polished optical fiber (SPOF) due to birefringence are investigated to characterize it by analyzing output intensities. As a novel method, polarization ellipses are analyzed to detect phase difference for different polarization angle according to the flat side of the planar side-polished region. And there is one more thing must be taking into consideration; since fibers are in the scale of micrometer, polishing fiber at the same way at every turn is almost impossible. Hence, if we want to use a SPOF for sensing refractive index exploiting polarization ellipses, firstly each of side-polished optical fibers to be used should be characterized in terms of polarization and phase difference separately.

1.1. Side-Polished Optical Fiber and Evanescent Field

In the sense of ray approach, light is guided in optical fiber core the way by the well-known principle of total internal reflection (TIR) [10]. However, if we consider the wave nature of the light, the small part of guided light power leaks through the core-cladding interfaces and continue propagation through a power loss in the cladding. This leaked light is called as evanescent field. The fields in the core and cladding feed each other and construct a mode pattern. Employing this feature of the light is a very convenient way to manage guided light in the core.

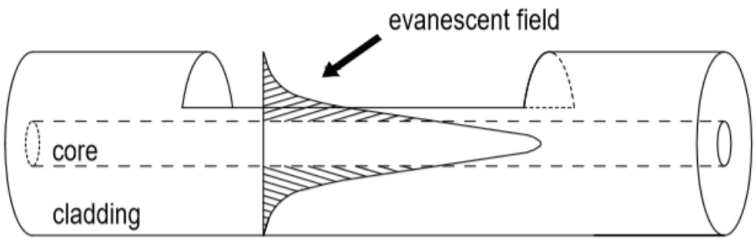

Figure 1.1. Side-polished optical fiber and evanescent field

By controlling evanescent field guided light properties can be changed [11-14]. To reach and control evanescent field, a section of the cladding next to core should be removed, because fibers are generally produced with thick cladding to inhibit attenuation caused by evanescent fields as much as possible. Removing a small part of cladding (generally planar and parallel to the core) of optical fiber process is called side-polishing and the fiber is called side-polished optical fiber or D-shaped optical fiber. In Figure 1.1 side-polished fiber and the evanescent field is illustrated. If removing part is planar all along the fiber, it is also called D-shaped optical fiber.

1.2. Fiber Optic Sensors

Usage of optical fiber sensors rapidly increases day by day in many areas such as medical industry, construction industry, aerospace industry, automotive industry etc. Its root cause is its excessive sensitivity capacity. Additionally, it offers high bandwidth, lightweight, low cost, ease to integrate into structures and invulnerable to interference with electromagnetic fields [15-29]. Depending on the application areas fiber optic sensors can be categorized as: physical sensors, chemical sensors, bio-medical sensors.

Among the many sensing quantities strain, temperature, pressure and refractive index sensing are the most popular ones. These quantities have been sensing with modified optical fiber like side-polished optical fiber by modulating intensity, polarization and phase shift between the modes at the sensing region of the optical fiber. In this thesis side-polished optical fiber is characterized based on its polarization and phase shift properties.

1.3. Birefringence Feature of a SPOF

Birefringence is the optical feature which occurs in anisotropic, transparent materials. Anisotropic medium in optics refers a medium which has non-uniform spatial distribution of dielectric constant. Upon light interacting with anisotropic media, vertical and horizontal polarized waves encounter different refractive indexes, and pass through the media with different angles and wavelengths so that speeds differ, as well [30-34].

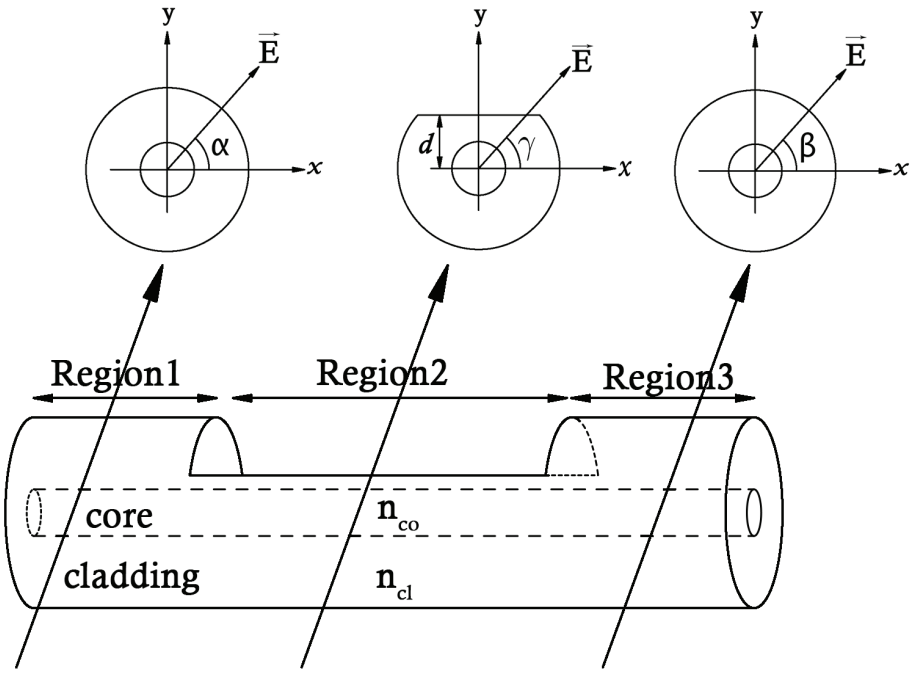

Figure 1.2. Side-polished optical fiber regions and the cross-sectional demonstrations

Propagating with different wavelengths leads phase difference between these two waves and they are called ordinary and extraordinary ray depending on the molecular structure of the material. The root cause is movement directions of the electrons in the

lattice. If the polarization direction of the light wave is in the same direction with the permitted movement direction of the electron, light tends to give some of its energy to the electron vibration, so the wave will be slowed down. According to the type of birefringent media, vibration direction could be either in single direction or both directions (vertical and horizontal) with exploiting different amount of energy. Consequently, at the output of the anisotropic medium, there will be a phase difference between the linearly polarized lights perpendicular to each other, unless light enters the medium in the direction of optical axes of birefringence.

If we divide SPOF into three regions, their names would be: The input side is region 1, the side-polished area is region 2 and the output side is region 3. In Figure 1.2, the regions and their cross-sections are illustrated. Since, in region 2 a part of cladding is removed, the side-polished are of optical fiber is anisotropic. Thus, SPOF is a birefringent device. The polarization property, and phase of the input light would change in region 2. In region 3 light propagates with the effects that occurred in region 2.

1.4. Overview of the Thesis

This thesis particularly deals with polarization and phase properties of the side-polished optical fiber. The prior motivation of the thesis is to improve the non-spectroscopic technique that figures out the SPOF effects on guided optical fiber modes. Besides, estimating mode content of a standard optical fiber outputs with matching simulation results is provided.

Chapter 2 includes explanation of optical waveguide theory. The exact cylindrical Maxwell solutions of circular optical fiber allow us to compute the intensity distributions of the Linearly Polarized LP modes. The theory of guided modes, radiation modes, LP mode formations and brief explanation of the modes of the side-polished region provide a theoretical background for understanding further chapters.

Chapter 3 contains discussion of mode orthogonality relation and the mode coupling theory. From this discussion we can interpret the polarization rotation effects of the perturbed optical fiber.

In Chapter 4, the computational model of experiments is formulated via Jones Matrix. Polarization and phase effect of the model is explained in detail. Also, calculation of elliptical polarization expressed mathematically.

In Chapter 5, experimental setups are introduced. Besides, parameters of the setups and procedure are determined.

In Chapter 6, all of the results and presented works are discussed. Initially, mode content estimation exploiting simulation results are explained. Next, the method of detecting polarization states and phase shifts is described.

Finally, in Chapter 7, whole results are interpreted. The benefits of this work and how it will be improved in future work are discussed.

CHAPTER 2

MODES OF SIDE-POLISHED OPTICAL FIBER

In this chapter, we start with electromagnetic analysis of a circular fiber mode fields that emerged from Maxwell's equations. Then we review polarization and phase effects of side-polished optical fiber on fundamental mode. According to these effects, theoretical discussions about polishing effects on degenerate fundamental modes are held.

2.1. Guided Modes of Circular Optical Fiber

Maxwell's equations lead us to solve cylindrical optical fiber electromagnetic fields, but even we use assumption of extending fiber cladding to infinity, it is excessively hard to solve with hand. Hence, in this thesis MATLAB is utilized in order to figure out mode fields and patterns.

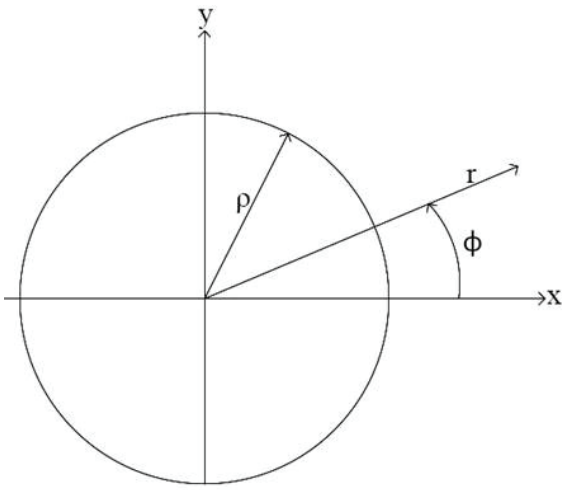

Figure 2.1. Demonstration of cross-sectional cartesian and cylindrical coordinate systems

In general perspective, 'mode' can be expressed as; Each of the (Maxwell equations) electromagnetic wave solutions depending on the geometry and optical properties [35-38]. There are finite number of guided modes in the core and infinite number of radiation modes in the cladding. The number of guided modes can be arranged by physical

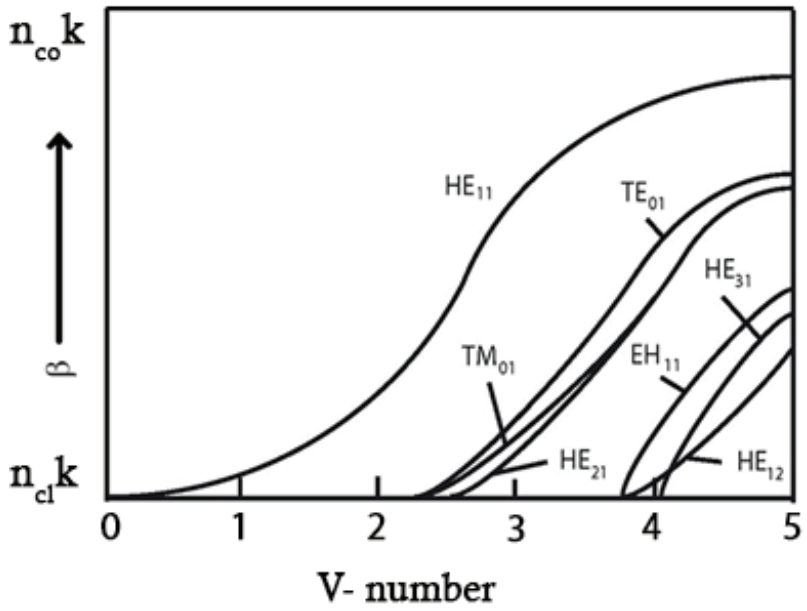

Figure 2.2. Cut-off frequencies $V - number$ of first seven TE, TM, HE and EH modes with respect to propagation constant β [22]

properties of the optical fiber, i.e., refractive indexes of materials and the cross-sectional geometry with light source's wavelength (λ) [10]. From these parameters we can deduce two dimensionless $modal\ parameters$ that are:

$$U = \rho(k^2 n_{co}^2 - \beta^2)^{1/2} \tag{2.1}$$

$$W = \rho(\beta^2 - k^2 n_{cl}^2)^{1/2} \tag{2.2}$$

where β is propagation constant, ρ is radii of core (see Figure 2.1), n_{co} is refractive index of core, n_{cl} is refractive index of cladding and $k = 2\pi/\lambda$ is wavenumber in free space. If we combine these two modal parameters:

$$V^2 = U^2 + W^2 \tag{2.3}$$

This quadratic summation gives us a new parameter:

$$V = \rho k(n_{co}^2 - n_{cl}^2)^{1/2} \tag{2.4}$$

which is called as $V - number$ or can be considered as cut-off frequency (normalized frequency). The parameter in the above brackets is $numerical\ aperture$:

$$NA = (n_{co}^2 - n_{cl}^2)^{1/2}, \tag{2.5}$$

and $profile\ height\ parameter$ is defined as:

$$\Delta = \frac{1}{2}\left\{1 - \frac{n_{cl}^2}{n_{co}^2}\right\} \tag{2.6}$$

According to $V-number$ we can understand which modes will propagate in optical fiber. Higher order modes can be suppressed by reducing core diameter and refractive index gap between core and cladding. This range of bound modes can be formulated by $V-number$ and $modal\ parameters$:

$$0 \leqslant U < V; \qquad 0 < W \leqslant V, \tag{2.7}$$

or propagation constant:

$$n_{cl}k < \beta \leqslant n_{co}k. \tag{2.8}$$

If mode parameters exist in these intervals, the mode will be a guided mode (or bound mode) which means permitted to guide in optical fiber core, if not, will be radiation mode.

Due to the wave features of the rays which are suffered from TIR in the core, there only finite number of guided modes exist. Figure 2.2 shows cut-off frequencies of the guided modes that are: hybrid and transverse modes. In this thesis only step-profile fibers are concerned. Its particular property is that core and cladding have uniform refractive index profiles among themselves:

$$n(r) = n_{co}, \quad 0 \leqslant r < \rho; \quad n(r) = n_{cl}, \quad \rho < r < \infty \tag{2.9}$$

To express modal fields we use cylindrical polar coordinates r, ϕ, z. We can write them in the separable forms:

$$\mathbf{E}(r,\phi,z) = \mathbf{e}(r,\phi)exp(i\beta z); \qquad \mathbf{H}(r,\phi,z) = \mathbf{h}(r,\phi)exp(i\beta z) \tag{2.10}$$

Expressions which are written bolt font indicate that it is a vector. We define $\mathbf{e}_r$, $\mathbf{e}_\phi$, $\mathbf{h}_r$, $\mathbf{h}_\phi$ as transverse field components and $\mathbf{e}_z$, $\mathbf{h}_z$ as longitudinal field components. Let ψ represents longitudinal field components, then ψ provides:

$$\left\{\frac{\partial^2}{\partial R^2} + \frac{1}{R}\frac{\partial}{\partial R} + \frac{1}{R^2}\frac{\partial^2}{\partial \phi^2} + U^2\right\}\psi = 0; \quad 0 \leqslant R < 1, \tag{2.11}$$

$$\left\{\frac{\partial^2}{\partial R^2} + \frac{1}{R}\frac{\partial}{\partial R} + \frac{1}{R^2}\frac{\partial^2}{\partial \phi^2} - W^2\right\}\psi = 0; \quad 1 < R < \infty, \tag{2.12}$$

where $R = r/\rho$ is normalized radii. When we solve cylindrical waveguide Maxwell equations, Bessel functions are emerging. Separable modal field solutions vary by region; $J_\nu(UR)cos(\nu\phi)$ or $J_\nu(UR)sin(\nu\phi)$ in the core, and $K_\nu(WR)cos(\nu\phi)$ or $K_\nu(WR)sin(\nu\phi)$ in the cladding, where $\nu \in N$ is mode index. The J_ν denotes Bessel function of the first kind and K_ν denotes Bessel function of the second kind. To generate the exact modal fields, we begin with selecting longitudinal components:

$$\mathbf{e}_z = A\frac{J_\nu(UR)}{J_\nu(U)}f_\nu(\phi), \quad \mathbf{h}_z = B\frac{J_\nu(UR)}{J_\nu(U)}g_\nu(\phi), \quad 0 \leqslant R < 1, \tag{2.13}$$

$$\mathbf{e}_z = A\frac{K_\nu(WR)}{K_\nu(W)}f_\nu(\phi), \quad \mathbf{h}_z = B\frac{K_\nu(WR)}{K_\nu(W)}g_\nu(\phi), \quad 1 < R < \infty, \tag{2.14}$$

where A and B are constants and f_ν, g_ν are the functions that determine the mode is whether even or odd (See Table 2.1). Now we can deduce the transverse fields from longitudinal components

$$\mathbf{e}_t = \frac{i}{k^2n^2 - \beta^2}\left\{\beta\nabla_t e_z - \left(\frac{\mu_0}{\epsilon_0}\right)^{1/2} k\hat{\mathbf{z}} \times \nabla_t h_z\right\}, \tag{2.15}$$

$$\mathbf{h}_t = \frac{i}{k^2n^2 - \beta^2}\left\{\beta\nabla_t h_z + \left(\frac{\epsilon_0}{\mu_0}\right)^{1/2} kn^2\hat{\mathbf{z}} \times \nabla_t e_z\right\}, \tag{2.16}$$

where $n = n(x, y)$ and,

$$k^2n^2 - \beta^2 = k^2n_{co}^2 - \beta^2 = U^2/\rho^2, \quad core, \tag{2.17}$$

$$k^2n^2 - \beta^2 = k^2n_{cl}^2 - \beta^2 = -W^2/\rho^2, \quad cladding. \tag{2.18}$$

These transverse fields leads the radial and azimuthal field components that are:

$$e_r = \frac{i}{p}\left\{\beta\frac{\partial e_z}{\partial r} + \left(\frac{\mu_0}{\epsilon_0}\right)^{1/2}\frac{k}{r}\frac{\partial h_z}{\partial \phi}\right\}, \tag{2.19}$$

$$e_\phi = \frac{i}{p}\left\{\frac{\beta}{r}\frac{\partial e_z}{\partial \phi} - \left(\frac{\mu_0}{\epsilon_0}\right)^{1/2} k\frac{\partial h_z}{\partial r}\right\}, \tag{2.20}$$

$$h_r = \frac{i}{p}\left\{\beta\frac{\partial h_z}{\partial r} - \left(\frac{\epsilon_0}{\mu_0}\right)^{1/2}\frac{kn^2}{r}\frac{\partial e_z}{\partial \phi}\right\}, \tag{2.21}$$

$$h_\phi = \frac{i}{p}\left\{\frac{\beta}{r}\frac{\partial h_z}{\partial \phi} + \left(\frac{\epsilon_0}{\mu_0}\right)^{1/2} kn^2\frac{\partial e_z}{\partial r}\right\}, \tag{2.22}$$

where $p = k^2n^2 - \beta^2$ and $n = n(r)$. These all fields are continuous along the core-cladding interface. Cylindrical field components of HE, EH modes (hybrid modes) shown in Table 2.1 on page 10, mode field components of TE, TM (transverse modes) modes shown in Table 2.2 on page 11 and in Table 2.3 on page 12 the hybrid mode variables are defined [10]. Circular fiber mode simulations are held by these formulations on MATLAB.

When optical fiber excited, each mode carries power. For lossless optical fiber power flows along the fiber axis, for jth mode intensity or time-averaged Poynting vector S_j is

$$S_j = \frac{1}{2}\Re\{\mathbf{E}_j \times \mathbf{H}_j^* \cdot \hat{\mathbf{z}}\} \tag{2.23}$$

where $\Re$ denotes real part of the expression. Thus we obtain

$$(\beta/|\beta|)P_j = \frac{1}{2}\int_{-\infty}^{\infty}\int_{-\infty}^{\infty} \mathbf{e}_j \times \mathbf{h}_j^* \cdot \hat{\mathbf{z}}\, dx\, dy \tag{2.24}$$

where P_j denotes power belongs to jth mode.

Table 2.1. Cylindrical field components of HE and EH modes of step-profile fiber

Components	*Core*	*Cladding*
e_r	$-\dfrac{a_1 J_{\nu-1}(UR)+a_2 J_{\nu+1}(UR)}{J_\nu(U)} f_\nu(\phi)$	$-\dfrac{U}{W}\dfrac{a_1 K_{\nu-1}(WR)-a_2 K_{\nu+1}(WR)}{K_\nu(W)} f_\nu(\phi)$
e_ϕ	$-\dfrac{a_1 J_{\nu-1}(UR)-a_2 J_{\nu+1}(UR)}{J_\nu(U)} g_\nu(\phi)$	$-\dfrac{U}{W}\dfrac{a_1 K_{\nu-1}(WR)+a_2 K_{\nu+1}(WR)}{K_\nu(W)} g_\nu(\phi)$
e_z	$\dfrac{-iU}{\rho\beta}\dfrac{J_\nu(UR)}{J_\nu(U)} f_\nu(\phi)$	$\dfrac{-iU}{\rho\beta}\dfrac{K_\nu(UR)}{K_\nu(U)} f_\nu(\phi)$
h_r	$\left(\dfrac{\epsilon_0}{\mu_0}\right)^{1/2}\dfrac{kn_{co}^2}{\beta}\dfrac{a_3 J_{\nu-1}(UR)-a_4 J_{\nu+1}(UR)}{J_\nu(U)} g_\nu(\phi)$	$\left(\dfrac{\epsilon_0}{\mu_0}\right)^{1/2}\dfrac{kn_{co}^2}{\beta}\dfrac{U}{W}\dfrac{a_5 K_{\nu-1}(WR)+a_6 K_{\nu+1}(WR)}{K_\nu(W)} g_\nu(\phi)$
h_ϕ	$-\left(\dfrac{\epsilon_0}{\mu_0}\right)^{1/2}\dfrac{kn_{co}^2}{\beta}\dfrac{a_3 J_{\nu-1}(UR)+a_4 J_{\nu+1}(UR)}{J_\nu(U)} f_\nu(\phi)$	$-\left(\dfrac{\epsilon_0}{\mu_0}\right)^{1/2}\dfrac{kn_{co}^2}{\beta}\dfrac{U}{W}\dfrac{a_5 K_{\nu-1}(WR)-a_6 K_{\nu+1}(WR)}{K_\nu(W)} f_\nu(\phi)$
h_z	$-i\left(\dfrac{\epsilon_0}{\mu_0}\right)^{1/2}\dfrac{UF_2}{k\rho}\dfrac{J_\nu(UR)}{J_\nu(U)} g_\nu(\phi)$	$-i\left(\dfrac{\epsilon_0}{\mu_0}\right)^{1/2}\dfrac{UF_2}{k\rho}\dfrac{K_\nu(UR)}{K_\nu(U)} g_\nu(\phi)$

Table 2.2. Cylindrical field components of TE and TM modes of step-profile fiber

TE Modes			TM Modes		
$Components$	$Core$	$Cladding$	$Components$	$Core$	$Cladding$
e_ϕ	$\dfrac{-J_1(UR)}{J_1(U)}$	$\dfrac{-K_1(WR)}{K_1(W)}$	e_r	$\dfrac{J_1(UR)}{J_1(U)}$	$\dfrac{n_{co}^2}{n_{cl}^2}\dfrac{K_1(WR)}{K_1(W)}$
h_r	$\left(\dfrac{\epsilon_0}{\mu_0}\right)^{1/2}\dfrac{\beta}{k}\dfrac{J_1(UR)}{J_1(U)}$	$\left(\dfrac{\epsilon_0}{\mu_0}\right)^{1/2}\dfrac{\beta}{k}\dfrac{K_1(WR)}{K_1(W)}$	e_z	$\dfrac{iU}{\rho\beta}\dfrac{J_0(UR)}{J_1(U)}$	$\dfrac{-in_{co}^2}{n_{cl}^2}\dfrac{W}{\rho\beta}\dfrac{K_0(WR)}{K_1(W)}$
h_z	$i\left(\dfrac{\epsilon_0}{\mu_0}\right)^{1/2}\dfrac{U}{k\rho}\dfrac{J_0(UR)}{J_1(U)}$	$-i\left(\dfrac{\epsilon_0}{\mu_0}\right)^{1/2}\dfrac{W}{k\rho}\dfrac{K_0(WR)}{K_1(W)}$	h_ϕ	$\left(\dfrac{\epsilon_0}{\mu_0}\right)^{1/2}\dfrac{kn_{co}^2}{\beta}\dfrac{J_1(UR)}{J_1(U)}$	$\left(\dfrac{\epsilon_0}{\mu_0}\right)^{1/2}\dfrac{kn_{co}^2}{\beta}\dfrac{K_1(WR)}{K_1(W)}$
$e_r = e_z = h_\phi = 0$			$e_\phi = h_r = h_z = 0$		

Table 2.3. Expansion of the hybrid mode variables

$f_\nu(\phi) = cos(\nu\phi); \quad g_\nu(\phi) = -sin(\nu\phi) \qquad even\ modes$ $f_\nu(\phi) = sin(\nu\phi); \quad g_\nu(\phi) = cos(\nu\phi) \qquad odd\ modes$	$F_1 = \left(\frac{UW}{V}\right)^2 \frac{b_1 + (1-2\Delta)b_2}{\nu}; \qquad F_2 = \left(\frac{V}{UW}\right)^2 \frac{\nu}{b_1 + b_2}$
$a_1 = \frac{F_2 - 1}{2}; \qquad a_3 = \frac{F_1 - 1}{2}; \qquad a_5 = \frac{F_1 - 1 + 2\Delta}{2}$	$b_1 = \frac{1}{2U}\left\{\frac{J_{\nu-1}(U)}{J_\nu(U)} - \frac{J_{\nu+1}(U)}{J_\nu(U)}\right\}$
$a_2 = \frac{F_2 + 1}{2}; \qquad a_4 = \frac{F_1 + 1}{2}; \qquad a_6 = \frac{F_1 + 1 - 2\Delta}{2}$	$b_2 = -\frac{1}{2W}\left\{\frac{K_{\nu-1}(W)}{K_\nu(W)} + \frac{K_{\nu+1}(W)}{K_\nu(W)}\right\}$

2.2. Radiation Modes of Circular Optical Fiber

A circular fiber can support guided (bound) modes if equation 2.8 is satisfied. However, there must exist other Maxwell's solutions to reach complete set of mode solutions [10]. In fact these kind of modes do exist, and they are radiation modes. Guided modes and radiation modes together construct a complete orthogonal set. This set can be express via series expansions of guided modes plus integral summation of radiation modes [37].

If we envision a plane wave coming from infinite distance that runs into waveguide core, undoubtedly a portion of the wave will be reflected at the one of the core boundary (TIR), while the rest of refracts and penetrates through the core and travels as a plane wave at the other side of the core. Reflection and refraction directions of these waves can be found by applying Snell's law. Now think a plane wave coming from above to the core. It results in transmitted wave below the core and reflected wave above the core. Thus the reflected waves are standing waves. These radiation fields are the solutions of Maxwell Equations and satisfy the core-cladding boundary conditions. Therefore, in every respect, the radiation field describes as a mode, unless it doesn't go through total internal reflection (TIR). This type of modes are called as radiation modes. Unlike guided modes, their propagation constants β are continuous and there is no restrictions on angle of incident plane wave.

For radiation modes, propagation constant is described in the interval:

$$-n_{cl}k \leqslant \beta \leqslant n_{cl}k \tag{2.25}$$

and imaginary propagation constants of evanescent modes have continuous spectrum in the range:

$$-i\infty < \beta < i\infty \tag{2.26}$$

These set of modes are identified with the parameter:

$$\zeta = (n_{cl}^2 k^2 - \beta^2)^{1/2} \tag{2.27}$$

in the range of

$$0 \leqslant \zeta < \infty. \tag{2.28}$$

Since radiation modes have a continuous spectrum, they cannot be normalized concerning a limited amount of power. If we derive the power expression of equation 2.24 for the radiation modes, integral diverges. To fix the normalization problem, we benefit

from dirac delta function. In place of equation 2.24, radiation mode power requires

$$\frac{1}{2}\int_0^{2\pi}\int_0^{\infty}[\mathbf{E}(\zeta)\times\mathbf{H}^*(\zeta')]\cdot\mathbf{e}_z\; r\; dr\; d\phi = s_p(\beta^*/|\beta|)\; P\;\; \delta(\zeta-\zeta') \tag{2.29}$$

where P is positive and real.

Compered to Equation 2.24, new features are included in this equation. The electric and magnetic fields belong to different radiation modes. And this consequences of the difference is shown itself in the Dirac Delta Function. If the two modes are different then the integral vanishes, if both modes are the same the statement goes to infinity.

The term $\beta^*/|\beta|$ ensures that P remains positive for even backward propagating. If β is imaginary then the left-hand side of Equation 2.29 becomes imaginary. As we determined power is always real, there is no power flow along the z axis if β is imaginary. And s_p term is also used for keep P positive. Whenever β is real $s_p = 1$, but for imaginary β values we might have to make $s_p = -1$ to assure P is positive.

2.3. Linearly Polarized Modes and Their Combinations

Linearly polarized modes $(LP_{\nu m})$ of an optical fiber refer to the combinations of hybrid HE and EH, transverse electric TE and transverse magnetic TM modes which of them have a same cut-off frequency. Figure 2.2 shows the cut-off conditions of first seven modes with respect propagation constant β [10].

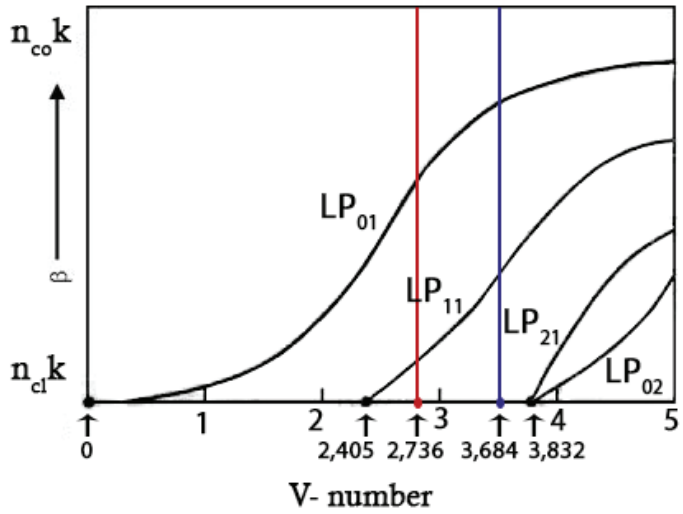

Figure 2.3. Cut-off frequencies $V - number$ of first four LP modes with respect to propagation constant β [22]

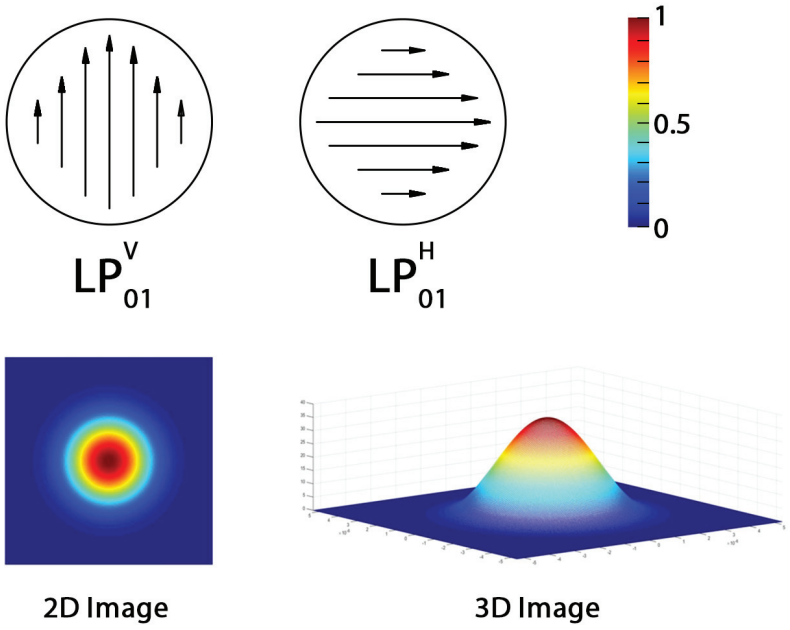

Figure 2.4. Symbolic electric field and simulated 2D / 3D intensity distributions of the LP_{01} modes

If we consider the components of the $LP_{\nu m}$ modes separately, they are not linearly polarized (except HE_{11}). However, when they combined, they construct linearly polarized modes. In this thesis only LP_{01} (fundamental mode) and LP_{11} modes being considered. Each LP modes have two degenerate forms that are perpendicular each other according to polarization state. The two polarization states called as $even$ and odd modes, e.g., vertical polarized LP_{01}^{V} and horizontal polarized LP_{01}^{H}. LP_{01} mode consists of just HE_{11} mode. For both even and odd form of LP_{01} modes' intensity distribution is the same, there is only one lobe in the middle (see Figure 2.4). In the intensity distribution of the LP_{11} mode, there are two lobes symmetrical with respect to the origin of the core. Also, the polarization directions of these lobes are $180°$ symmetrical to each other. The two lobes rotate according to the combination of hybrid and transverse modes. There are four possibility in formation of LP_{11} mode: horizontal polarized - horizontal oriented $LP_{11}^{HH} = even\ HE_{21} + TM_{01}$, vertical polarized - vertical oriented $LP_{11}^{VV} = even\ HE_{21} - TM_{01}$, vertical polarized - horizontal oriented $LP_{11}^{VH} = odd\ HE_{21} + TE_{01}$, horizontal polarized - vertical oriented $LP_{11}^{HV} = odd\ HE_{21} - TE_{01}$. In Figure 2.5, these combinations of LP_{11} modes are illustrated via symbolic electric field and simulated intensity distributions.

In the optical fiber, if $V - number$ is lower than 2.405, it means just fundamental mode is propagating, i.e., single-mode propagation. Also, if $V - number$ is lower

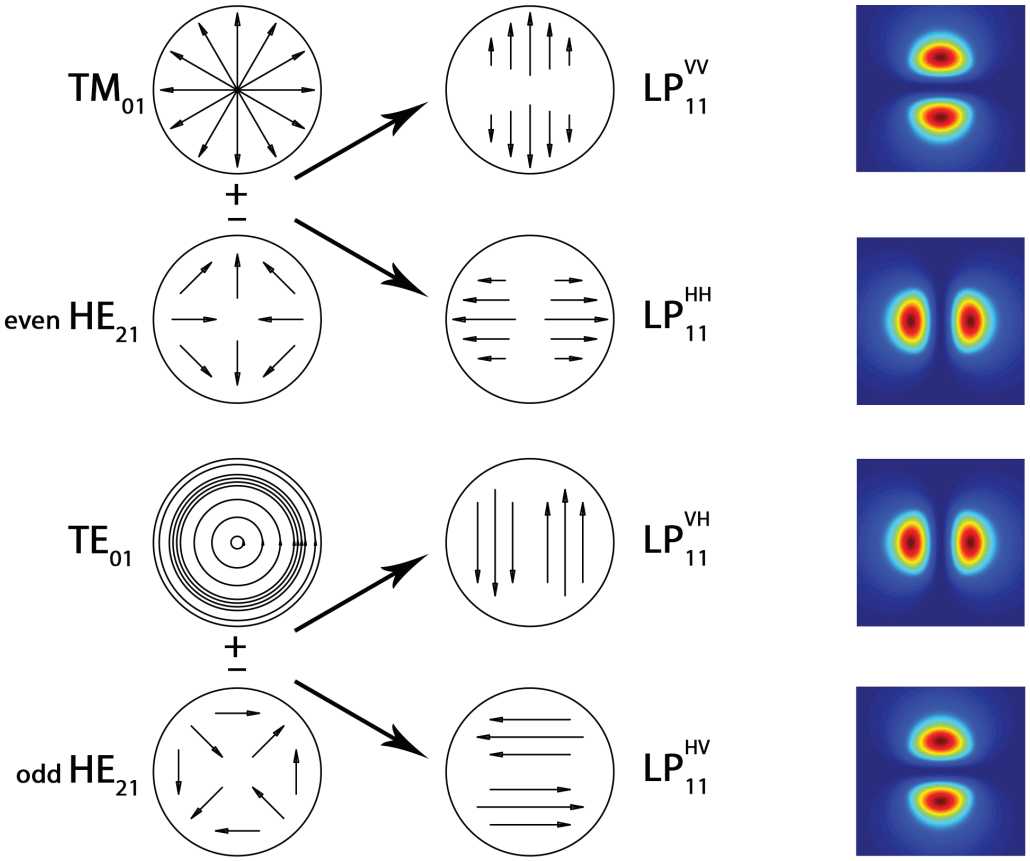

Figure 2.5. The combinations in terms of the symbolic electric field and simulated intensity distributions of the possible four type of LP_{11} modes

than 3.832, it means LP_{01} mode and LP_{11} mode is propagating together, i.e., two-mode propagation. In Figure 2.3 the cut-off frequency of first four LP modes are illustrated.

2.4. Modes in the Side-Polished Region of a SPOF

The previous derivations for mode fields are performed under the condition of extending the cladding to infinity. And we assume the refractive indexes of the cladding and the core is uniform in everywhere [10]. In real, cladding region is limited and this situation leads attenuation for long distance transmission. For short distance transmission, the attenuation caused by the cladding that not extend to infinity is negligible. But, if we polish cladding near to core, then the attenuation would be non-negligible. Beside, attenuation at the polished region will not be uniform, because polishing process is planar, not circular. And also, after removing a part of cladding, refractive index of polished region will also change. This anisotropy causes birefringence. We can separate the SPOF structure

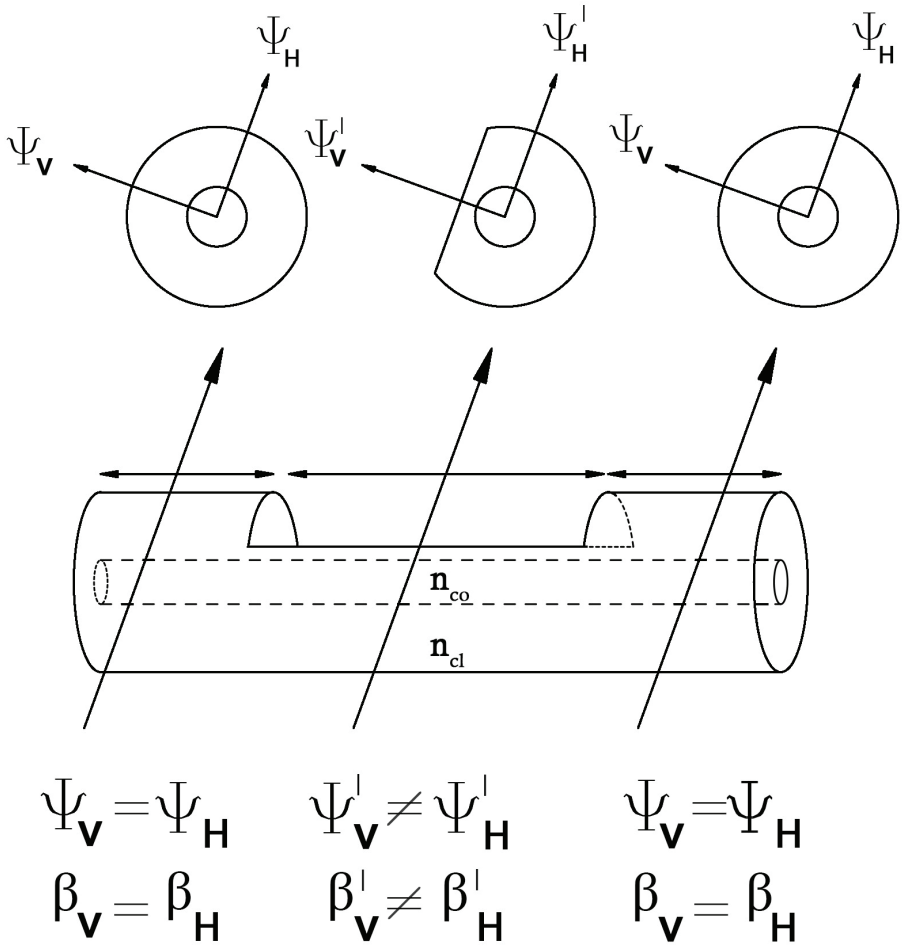

Figure 2.6. Demonstration of vertically and horizontally polarized modes by regions according to propagation constant relation

into 3 regions (see Figure 1.2). In region 1 there is no perturbation, so degenerate modes propagating without coupling to each other. Degenerate mode means that modes which have same propagation constant but perpendicularly polarized relative to each other, e.g., Ψ_H and Ψ_V (see Figure 2.6). Ψ_H denotes horizontally polarized and Ψ_V denotes vertically polarized modes. If degenerate modes don't face any imperfections, they propagate as a single mode, and their polarization directions construct a new state of polarization according to electric field amplitude contributions of two degenerate modes. In region 2, perturbation caused by side polishing breaks the degeneracy of the modes. Then $\Psi_H^{'}$ and $\Psi_V^{'}$ modes couple to each other. Based on the polishing effect a part of power of the guided modes also couple to radiation modes. This coupling to radiation modes cause loss in the core. At the same time according to optical axis of birefringence, there occur phase difference between the vertically and horizontally polarized modes. Eventually, at the region 3 side-polished region modes couple back to degenerate modes. However,

based on the losses and phase difference occurred in the region 2, linear polarized light at the input converts into the elliptically polarized light at the output.

To examine perturbation effects of side-polished optical fiber on the linearly polarized modes, we separately experimented two-mode propagation (LP_{01} and LP_{11}) and single-mode propagation. In two-mode propagation case, there occur coupling between degenerate modes and LP_{01} - LP_{11} modes at the same time. An occurrence of coupling between LP modes prevents us from examining the polarization and phase relation between input and output more precisely. When we use single-mode propagation, only degenerate fundamental modes are coupled to each other. Therefore it is a more convenient method that uses single-mode propagation to analyze polarization and phase properties of the SPOF.

CHAPTER 3

MODE COUPLING

3.1. Orthogonality of Modes

All of the optical fiber modes are mutually orthogonal in perfect optical fiber [37]. Orthogonality is described by aid of Equation 2.29. This equation is not only states the normalization but also orthogonality. If $E(\zeta)$ represent a guided or radiation mode's electric field and $H(\zeta')$ represent any other guided or radiation mode, then the integral of these modal fields' cross product vanishes. Only if both fields belong to same mode case makes the integral non zero. The terms ζ and ζ' are utilized to identify different modes. These terms might define guided or radiation modes. The Dirac delta function in the Equation 2.29 is valid if both ζ and ζ' indicate radiation modes. For guided modes, we have to replace Dirac delta function with Kronecker delta function, which is unity if both labels equal, otherwise zero. Now generalize the Equation 2.29 for all modes

$$\int_0^{2\pi} \int_0^{\infty} [\mathbf{E}_{j\mathrm{t}} \times \mathbf{H}^*_{k\mathrm{t}}] \cdot \mathbf{e}_z \; r \; dr \; d\phi = 2 s_p (\beta^* / |\beta|) \; P \; \delta_{jk} \tag{3.1}$$

where subscript 't' indicates transverse field, 'j' and 'k' denote different mode indexes and the symbol δ_{jk} specify Kronecker's delta function. We make inference from the orthogonality statement (3.1); if we sum powers carried by all of the modes, it gives us simply power carried by optical fiber field. Integrating Poynting vector over infinite cross-section and sum of the powers carried by all modes (superposition) are same things that gives total power carried by optical fiber.

In perturbed optical fiber, e.g., side-polished optical fiber, modes are not orthogonal to each other anymore. If modes are not orthogonal, then the modes couple to each other. For SPOF in the region 1 modes are orthogonal to each other. The region 2 is side-polished, thus this perturbation breaks the mode orthogonality. In this region the modes couple to each other. Finally at the region 3, mode orthogonality re-emerges.

3.2. Mode Coupling Caused by Perturbation

In the beginning of previous chapter, we studied Maxwell solutions of the guided modes. These modes can propagate for long distances along the optical fiber axis without any distortion if the waveguide is straight and homogeneous. In real, waveguides haven't got a perfect structure. There are imperfections like refractive index inhomogeneities and variations of the core diameter. And these imperfections lead coupling the modes among each other; namely energy transfer between the modes [37-41]. For our case, we call the imperfection caused by the polished region of fiber as a perturbation. Thus, in this thesis we deal with the mode coupling by cause of the SPOF's perturbation.

Now consider side-polished optical fiber, there is imperfection of refractive index inhomogeneity at the polished area. Extracted region's refractive index is no longer n_{cl} but the refractive index of the external medium n_{ex} (see Figure 3.1). Due to change in refractive index we can define refractive index by

$$n = n(x, y, z). \tag{3.2}$$

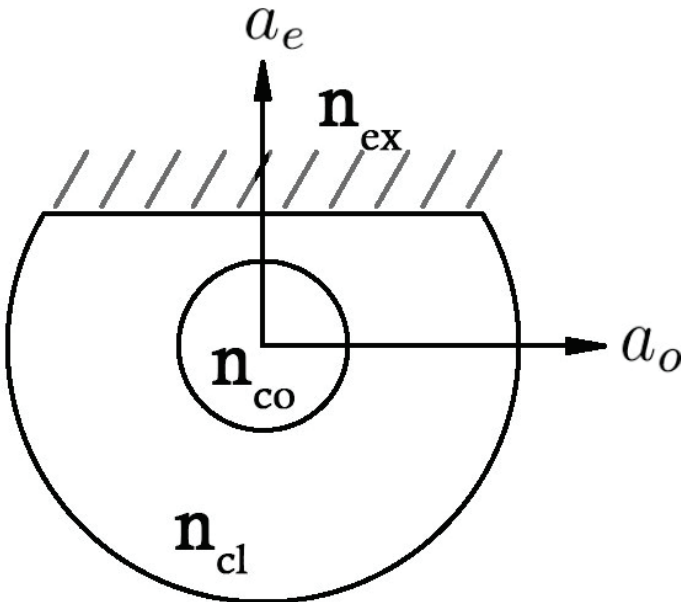

Figure 3.1. Demonstration of external medium refractive index n_{ex} and birefringence axises of SPOF, i.e, extraordinary a_e and ordinary a_o axises

We also express the propagation constant β via functions of the modal fields

$$\beta_j = \left(\frac{\mu_0}{\epsilon_0}\right)^{1/2} k \left(\frac{\displaystyle\int_{A_\infty} n^2 \, \mathbf{e}_j \times \mathbf{h}_j^* \cdot \hat{\mathbf{z}} \, \mathrm{d}A}{\displaystyle\int_{A_\infty} n^2 \, |\mathbf{e}_j|^2 \, \mathrm{d}A} \right) \tag{3.3}$$

where A_∞ determines infinite cross section and j determines modal indice. If we separate modal field components into transverse and longitudinal

$$\mathbf{E} = \mathbf{E}_\mathrm{t} + E_z \hat{\mathbf{z}}; \qquad \mathbf{H} = \mathbf{H}_\mathrm{t} + H_z \hat{\mathbf{z}}, \tag{3.4}$$

where all field components are z dependent. Now we define the operator ∇

$$\nabla = \nabla_\mathrm{t} + \hat{\mathbf{z}} \, \partial/\partial z \tag{3.5}$$

where ∇_t defined as:

$$\nabla_\mathrm{t} \Psi = \hat{\mathbf{x}} \frac{\partial \Psi}{\partial x} + \hat{\mathbf{y}} \frac{\partial \Psi}{\partial y} \tag{3.6}$$

Applying the equation 3.4 into the source free Maxwell equations and transverse components with eliminating longitudinal components

$$\mathbf{E}_\mathrm{t} = \frac{1}{kn^2} \left\{ i \left(\frac{\mu_0}{\epsilon_0}\right)^{1/2} \hat{\mathbf{z}} \times \frac{\partial \mathbf{H}_\mathrm{t}}{\partial z} + \frac{1}{k} \nabla_\mathrm{t} \times (\nabla_\mathrm{t} \times \mathbf{E}_\mathrm{t}) \right\}, \tag{3.7}$$

$$\mathbf{H}_\mathrm{t} = \frac{1}{k} \left\{ i \left(\frac{\epsilon_0}{\mu_0}\right)^{1/2} \hat{\mathbf{z}} \times \frac{\partial \mathbf{E}_\mathrm{t}}{\partial z} - \frac{1}{k} \nabla_\mathrm{t} \times \left(\frac{\nabla_\mathrm{t} \times \mathbf{H}_\mathrm{t}}{n^2} \right) \right\}. \tag{3.8}$$

Converting the field expansions into the form of:

$$\hat{\mathbf{e}}_{\mathrm{t}j} = -\frac{1}{kn^2} \left\{ \left(\frac{\mu_0}{\epsilon_0}\right)^{1/2} \beta_j \hat{\mathbf{z}} \times \hat{\mathbf{h}}_{\mathrm{t}j} - \frac{1}{k} \nabla_\mathrm{t} \times (\nabla_\mathrm{t} \times \hat{\mathbf{e}}_{\mathrm{t}j}) \right\}, \tag{3.9}$$

$$\hat{\mathbf{h}}_{\mathrm{t}j} = \frac{1}{k} \left\{ \left(\frac{\epsilon_0}{\mu_0}\right)^{1/2} \beta_j \hat{\mathbf{z}} \times \hat{\mathbf{e}}_{\mathrm{t}j} + \frac{1}{k} \nabla_\mathrm{t} \times \left(\frac{\nabla_\mathrm{t} \times \hat{\mathbf{h}}_{\mathrm{t}j}}{n^2} \right) \right\}. \tag{3.10}$$

Exact mode field expansions are described as

$$\mathbf{E}_\mathrm{t}(x, y, z) = \sum_j \{b_j(z) + b_{-j}(z)\} \, \hat{\mathbf{e}}_{\mathrm{t}j} \, (x, y, \beta_j(z)), \tag{3.11}$$

$$\mathbf{H}_\mathrm{t}(x, y, z) = \sum_j \{b_j(z) + b_{-j}(z)\} \, \hat{\mathbf{h}}_{\mathrm{t}j} \, (x, y, \beta_j(z)) \tag{3.12}$$

where subscript 't' determines the transverse components of the fields, 'j' denotes forward propagating modes, '$-j$' denotes backward propagating modes and $b_j(z)$ defines

the modal amplitude and the phase. Note that summation includes both guided and radiation modes.

$$b_{\pm j}(z) = a_{\pm j}(z) exp\left\{\pm i \int_0^z \beta_j(z) dz\right\} \tag{3.13}$$

where the propagation constant β_j and the field components of any modes satisfy the Equations 3.11 and 3.12 for any position of z along the fiber. If we combine the Equations 3.9, 3.10, 3.11 3.12, and orthogonality relation 3.1, it leads

$$\frac{\mathrm{d}b_j}{\mathrm{d}z} - \frac{\mathrm{d}b_{-j}}{\mathrm{d}z} - i\beta_j(b_j + b_{-j}) = -\frac{1}{2}\sum_k (b_k - b_{-k}) \int_{A_\infty} \hat{\mathbf{e}}_j \times \frac{\partial \hat{\mathbf{h}}_k}{\partial z} \cdot \hat{\mathbf{z}}\, \mathrm{d}A, \tag{3.14}$$

$$\frac{\mathrm{d}b_j}{\mathrm{d}z} + \frac{\mathrm{d}b_{-j}}{\mathrm{d}z} - i\beta_j(b_j - b_{-j}) = \frac{1}{2}\sum_k (b_k + b_{-k}) \int_{A_\infty} \hat{\mathbf{h}}_j \times \frac{\partial \hat{\mathbf{e}}_k}{\partial z} \cdot \hat{\mathbf{z}}\, \mathrm{d}A, \tag{3.15}$$

where subscripts 'j' and 'k' denote mode indices. We don't write the subscript 't' anymore, because integration is valid for only the transverse components of the modal fields. If we add and subtract equations 3.14 and 3.15 , it gives us:

$$\frac{\mathrm{d}b_j}{\mathrm{d}z} - i\beta_j\, b_j = \sum_k \left\{C_{jk}\, b_k + C_{j-k}\, b_{-k}\right\}, \tag{3.16}$$

$$\frac{\mathrm{d}b_{-j}}{\mathrm{d}z} + i\beta_j\, b_{-j} = -\sum_k \left\{C_{-jk}\, b_k + C_{-j-k}\, b_{-k}\right\}, \tag{3.17}$$

where the C_{jk}, C_{-jk}, C_{j-k}, C_{-j-k} are the coupling coefficient of forward and backward propagating modes defined by

$$C_{jk} = \frac{1}{4}\int_{A_\infty} \left\{\hat{\mathbf{h}}_j \times \frac{\partial \hat{\mathbf{e}}_k}{\partial z} - \hat{\mathbf{e}}_j \times \frac{\partial \hat{\mathbf{h}}_k}{\partial z}\right\} \cdot \hat{\mathbf{z}}\, \mathrm{d}A, \qquad j \neq k; \qquad C_{jj} = 0. \tag{3.18}$$

Alternatively we can express the coupling coefficient in the more compact form

$$C_{jk} = \left(\frac{\epsilon_0}{\mu_0}\right)^{1/2} \frac{k}{4} \frac{1}{\beta_j - \beta_k} \int_{A_\infty} \hat{\mathbf{e}}_j^* \cdot \hat{\mathbf{e}}_k \frac{\partial n^2}{\partial z}\, \mathrm{d}A, \qquad j \neq k; \qquad C_{jj} = 0. \tag{3.19}$$

3.3. Mode Polarization Rotation at Side-Polished Optical Fiber

LP modes mentioned in Section 2.3 are linearly polarized modes, as the name implies. In the unperturbed fiber, light could sustain linearity of polarization. However, if the fiber has geometric deformations or perturbed regions, the light would not maintain its linear state of polarization. As shown in Figure 2.6 linearly polarized degenerate modes are propagating in region 1. However, at the region 2, perpendicularly polarized

modes suffer from mode coupling, attenuation, and phase shifts [42-45]. For each mode, different amount of energy couples and phase shift occurs. This situation breaks linearity of polarization at the region 3. The polarization change through the side-polished region can be called as a coupling between orthogonally polarized modes.

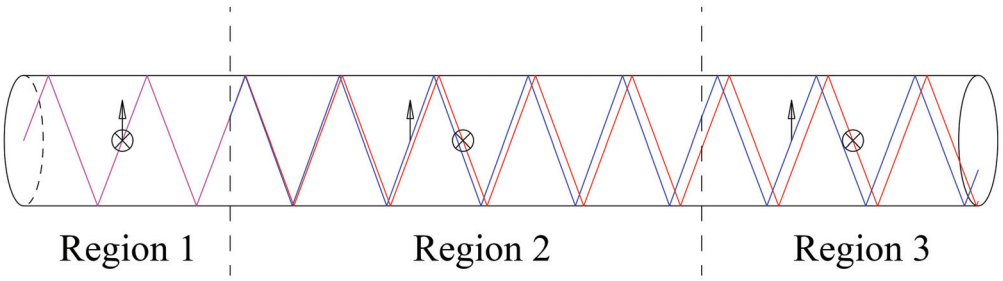

Figure 3.2. An occurrence of a phase difference between horizontally and perpendicularly polarized modes

There are always two states of polarization for each LP modes that are perpendicular to each other. For SPOF we set the ordinary axis a_o as parallel and extraordinary axis a_e as perpendicular polarization (see Figure 3.1). The coupling coefficient equation 3.19 tells us electric fields of orthogonal modes cannot couple to each other in an isotropic medium. When two orthogonally polarized modes are applied to Equation 3.19, dot product of two perpendicularly polarized transverse electric fields vanishes and only the longitudinal electric field components e_z are contributed to integral.

Moreover, this anisotropy causes slightly differing the propagation constants which belong to the similar mode but perpendicular polarized to each other. The difference between the propagation constants of the two orthogonally polarized similar modes, i.e., LP_{01} vertically polarized and LP_{01} horizontally polarized, generates phase shift among them. Figure 3.2 shows how phase shift arises at the side-polished region. In the sense of ray approach, the distinction between two modes which have different propagation constant is reflection angle at the core-cladding boundary. In region 1 degenerate modes propagate in phase. In region 2, phase shifts for each modes occur. In region 3, the degenerate modes propagate with constant phase difference. Thus, if we combine occurrence of different loss amount and phase shift between quasi-degenerate modes at the side-polished region, there originates mode polarization rotation at the output, i.e., elliptically polarized light.

CHAPTER 4

COMPUTATIONAL MODEL OF SIDE-POLISHED OPTICAL FIBER COUPLED DEVICE STRUCTURE

4.1. Computational Model of the Device

Side-polished optical fiber breaks the circular symmetry from the beginning of the region 2, and fiber turns into symmetrical form at the beginning of the region 3 (see Figure 1.2). This asymmetric structure causes to occur birefringence. Therefore there emerges extraordinary and ordinary axis at the SPOF (see Figure 3.1). We define the phase shifts generated by the birefringent SPOF extraordinary and ordinary axises as $\delta\varphi_e$ and $\delta\varphi_o$ respectively. At the same time, according to anisotropy of the SPOF guided modes would couple to radiation modes at a certain level. To specify loss caused by coupling, we define attenuation coefficients as α_e and α_o respectively.

We can mathematically model the device with Jones Matrix method [9]. Let separate the whole system in three regions with the matrices of M1, M2 and M3, these matrices represent input, SPOF and the linear polarizer respectively. We decide the laboratory axis as horizontal plane, and describe the output electric field with orthogonal components, i.e., E_{out}^{H} and E_{out}^{V}. So the mathematical model is

$$\begin{pmatrix} E_{out}^{H} \\ E_{out}^{V} \end{pmatrix} = \mathrm{M3} \cdot \mathrm{M2} \cdot \mathrm{M1}. \tag{4.1}$$

With respect to laboratory axis we can rotate the laser, i.e., polarization direction of the input (M1)

$$\mathrm{M1} = \mathrm{R}(\Theta) \begin{pmatrix} 1 \\ 0 \end{pmatrix} \tag{4.2}$$

where Θ is the angle of the laser rotation according to laboratory axis and $\mathrm{R}(\Theta)$ is the rotation matrix

$$\mathrm{R}(\Theta) = \begin{pmatrix} \cos(\Theta) & -\sin(\Theta) \\ \sin(\Theta) & \cos(\Theta) \end{pmatrix}. \tag{4.3}$$

Our initial polarization direction is horizontal. We take the positive (+) sign of rotation as

clockwise direction. Orientation of the ordinary axis a_o according to input is unknown so we define M2

$$\mathrm{M2} = \mathrm{R}(-\Omega) \begin{pmatrix} e^{-i\Lambda-\alpha_o} & 0 \\ 0 & e^{i\Lambda-\alpha_e} \end{pmatrix} \mathrm{R}(\Omega) \tag{4.4}$$

where i denotes the imaginary unit, Ω is the angle between the laboratory axis and side-polished planar surface (a_o) and phase difference between two orthogonal modes is $\Lambda = \delta\varphi_e - \delta\varphi_0$. Finally Jones Matrix of the linear polarizer is described by

$$\mathrm{M3} = \begin{pmatrix} \cos^2(\zeta) & \cos(\zeta)\sin(\zeta) \\ \cos(\zeta)\sin(\zeta) & \sin^2(\zeta) \end{pmatrix} \tag{4.5}$$

where ζ is the rotation angle of the linear polarizer from laboratory axis in the counter-clockwise direction.

4.2. Polarization Rotation Properties of the Device

When side-polished optical fiber is manufactured, its birefringence and attenuation effects are unknown. To solve polarization and phase behaviour of the SPOF, we need to characterize it. The computational model of the characterization process is explained in the previous section. There are two parameter we can arrange in the input. First one is arranging guided mode number in the core. And the second one is rotating input polarization direction. To focus more on polarization and phase characterization we let only fundamental mode propagation.

Birefringence and attenuation effects on degenerate modes at the side-polished region are extremely depend on polarization direction of input light [9]. So, as seen in Equation 4.2 in M1 there is rotation matrix with respect to Θ. The angle of Θ determines the polarization direction of the input. However, the angle Ω between the input polarization direction and the ordinary axis a_o of the SPOF is unknown. Therefore in M2 (see Equation 4.4), we rotate Ω the input to be in line with the a_o axis and then rotate back $-\Omega$ degree to turn back to laboratory axis.

At the output, there is 360° rotatable linear polarizer. This is our third parameter which we can arrange. To detect polarization information of the outputs we used this polarizer at 10° intervals. Then we obtain polarization of ellipses. With solving the elliptical polarization equations (see Section 4.3), we found out the phase difference between parallel and perpendicular polarized modes.

4.3. Analytical Description of Polarization Ellipse

Polarization is a feature of electric field. It specify magnitude and direction of the vibrating electric field of a electromagnetic wave. In linear polarization there is no phase difference between the horizontal and vertical electric field components and direction is depend on the magnitudes of the electric field components. If there is phase a difference between the components, the polarization type would be elliptical polarization [42]. Circular polarization is the special case that phase difference is $90°$.

To evaluate phase difference between the horizontal and vertical electric field components from a polarization of ellipse, we first define the coordinates of ellipse: κ denotes the major axis and η denotes the minor axis. Laboratory axises are defined as x axis and y axis, horizontal and vertical axises respectively. Length of semi-major axis is a and length of semi-minor axis is b. When we fit the ellipse in the rectangular (see Figure 4.1), its coordinates are described as (a_1, a_2), $(a_1, -a_2)$, $(-a_1, -a_2)$ and $(-a_1, a_2)$. The angle γ which is measured counterclockwise from the major axis of the ellipsoid κ to the positive horizontal axis x states the orientation of the ellipse. γ can take the values between $0°$ and $180°$. χ is the shape parameter and $cos(\chi)$ is related with the eccentricity of the ellipse. It is the angle between the hypotenuse and semi-major axis on the triangle of the constructed by semi-major and semi-minor axis. χ can take the values between $-45°$ and $45°$. And ζ indicate the angle of the instantaneous electric field vector.

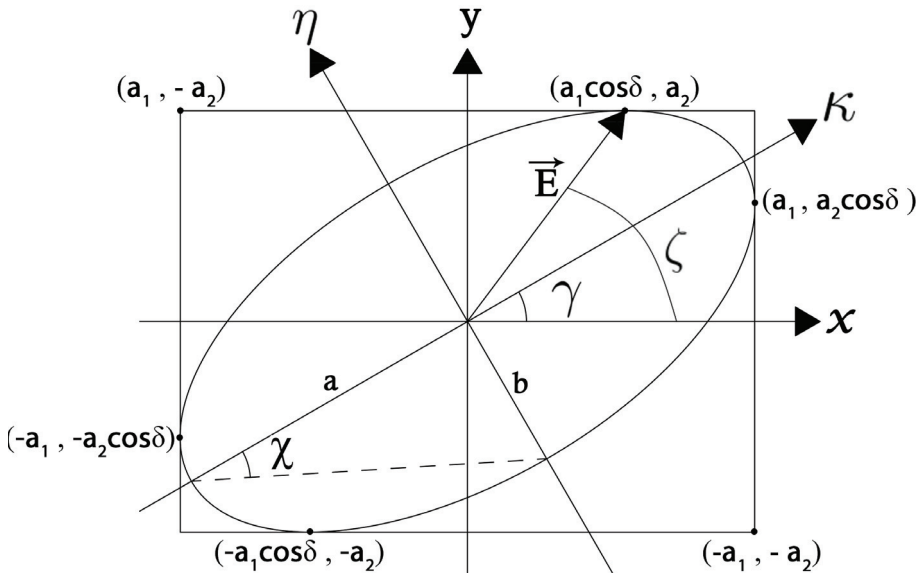

Figure 4.1. Sketch of elliptical polarization with the parameters

In the figure 4.1, an electric field vector $\overrightarrow{E}$ belongs to elliptical polarization is shown in a random time. Its components according to x axis and y axis are $E_x\hat{\mathrm{x}}$ and $E_y\hat{\mathrm{y}}$ respectively. Let define general elliptical polarization expression:

$$\left(\frac{E_x}{a_1}\right)^2 + \left(\frac{E_y}{a_2}\right)^2 - 2\left(\frac{E_x}{a_1}\right)\left(\frac{E_y}{a_2}\right) cos\gamma = sin^2\delta \tag{4.6}$$

where δ denotes phase difference between horizontal and vertical electric field components. These components are defined as

$$E_x = a_1 cos(\tau + \delta_1) \tag{4.7}$$

$$E_y = a_1 cos(\tau + \delta_2) \tag{4.8}$$

where τ represents reference phase degree, δ_1 is the phase of the E_x and δ_2 is the phase of the E_y. Thus, the phase difference δ is expressed via

$$\delta = \delta_1 - \delta_2. \tag{4.9}$$

Let convert the $x - y$ coordinates system into the $\kappa - \eta$ coordinate system

$$E_\kappa = E_x\ cos(\gamma) + E_y\ sin(\gamma) \tag{4.10}$$

$$E_\eta = E_x\ sin(\gamma) + E_y\ cos(\gamma). \tag{4.11}$$

Now the electric field components are

$$E_\kappa = a\ cos(\tau + \delta_0) \tag{4.12}$$

$$E_\eta = \pm b\ sin(\tau + \delta_0) \tag{4.13}$$

where δ_0 is the common phase of the electric field components of the $\kappa - \eta$ coordinate. Hence, as expected, in the coordinate system of the ellipse, there is no phase difference between E_κ and E_η. The relation between the axises of the ellipse and lengths of rectangular is

$$a^2 + b^2 = a_1^2 + a_2^2 \tag{4.14}$$

Finally we can deduce phase relation

$$\pm\ ab = a_1 a_2\ sin\delta. \tag{4.15}$$

For alternative forms, we ought to define

$$\frac{a_1}{a_2} = tan(\alpha); \qquad \frac{a}{b} = tan(\chi) \tag{4.16}$$

where α is the degree between diagonal of the rectangular and the y axis. Therefore the phase difference δ could be also found via

$$tan(2\gamma) = tan(2\alpha)cos(\delta) \tag{4.17}$$

or

$$sin(2\chi) = sin(2\alpha)sin(\delta). \tag{4.18}$$

Moreover the phase term $cos(\delta)$ is occur on the intersections of the ellipse and the rectangular (see Figure 4.1).

The last parameter is eccentricity. It is denoted by e and describes how circular the ellipse is. The formulation of e is:

$$e = \frac{\sqrt{a^2 - b^2}}{a}. \tag{4.19}$$

CHAPTER 5

EXPERIMENTAL STUDIES ON CHARACTERIZATION OF SIDE-POLISHED OPTICAL FIBER

In this chapter, experimental setups and the measurement technique are explained. Besides, the components of the experiment and their parameters also described.

5.1. Experimental Procedure

Two experimental setups were performed (see Figure 5.1 and 5.2). The whole system was placed on the optical table. First experiment was two-mode propagation and the other was the single-mode propagation experiment. For both experiments different lasers were used. In the cause of coupling laser output to the optical fiber input efficiently, a 20X convex lens was placed between the laser and the optical fiber input. Side-polished part of the step index optical fiber was approximately in the middle of the total length of the optical fiber. To arrange the number of modes propagating, we need the exact optical fiber parameters. As an optical fiber Corning HI 1060 was used. Its specifications are: refractive index of the core n_{co} = 1.464, numerical aperture NA = 0.14, core radius ρ = 2.65 μm, and the cladding radius is b = 62.5 μm according to data sheet of Corning HI1060 [46]. Planar side-polished region's core - fiber flat side distance is 9.32 + 2.65 μm. At the output of optical fiber a 360° rotatable linear polarizer was located. Measurements were obtained for every 10° rotation to create polarization ellipses. Intensity distributions were measured by a Charge Coupled Device (CCD) Camera which pixel size is 17 μm (H) $\times$ 11 μm (V).

5.2. Two-Mode Experiment

In the Figure 5.1 schematic demonstration of the experimental setup is sketched. As a light source He-Ne 632.8nm laser is used. According to the setup parameters $V - number$ is 3.684 (see Equation 2.4). When we place 3.684 in the Figure 2.3, left side of the blue line determines the supported modes. That are LP_{01} and LP_{11} modes.

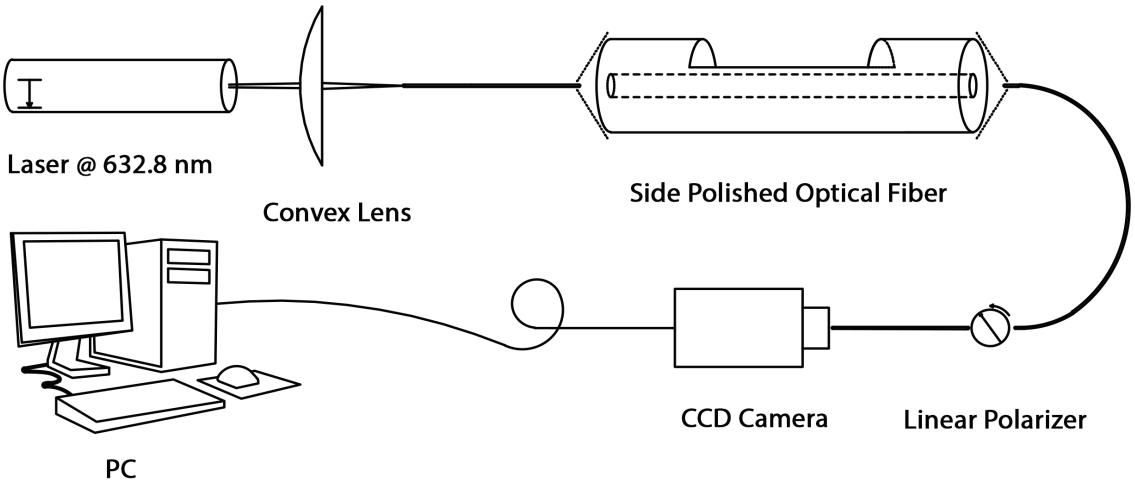

Figure 5.1. Schematic sketch of the two-mode experiment

Initially, the output of unpolished, i.e., output of standard optical fiber was checked with the linear polarizer. We reached that the output light is linearly polarized. Then we set the setup with the SPOF. To investigate mode content and the polarization properties of the SPOF, we measured the output for different angles of linear polarizer angles, e.g., $0°$, $45°$ and $90°$ according to laboratory axis. Also the polarization direction of the laser was $0°$, i.e., laboratory axis.

5.3. Single-Mode Experiment

In the Figure 5.2 schematic demonstration of the experimental setup is sketched. As a light source Cs 852nmn laser was used. According to the setup parameters $V - number$ is 2.736 (see Equation 2.4). When we place a line to the value of 2.736 on the horizontal axis in the Figure 2.3, it is seen there are still two modes propagating on the left side of red line. But LP_{11} mode is at the near of the cut-off frequency. To provide single-mode propagation at the side-polished region, we set the mode filter at the input side of the fiber (see Figure 5.2). The filtering method was bending the fiber. Consider total internal reflection (TIR) phenomena. If an optical fiber is perfectly straight, then the modes propagating in the core with constant reflection angle. When a ray comes to the normal of the core-cladding boundary with an angle higher than the critical angle, it would radiate through the boundary. However, bending makes the reflection angle increase. Since the reflection angle also increases as the cut-off frequency of the mode increases, when we bend the optical fiber enough, the earlier radiated mode would be

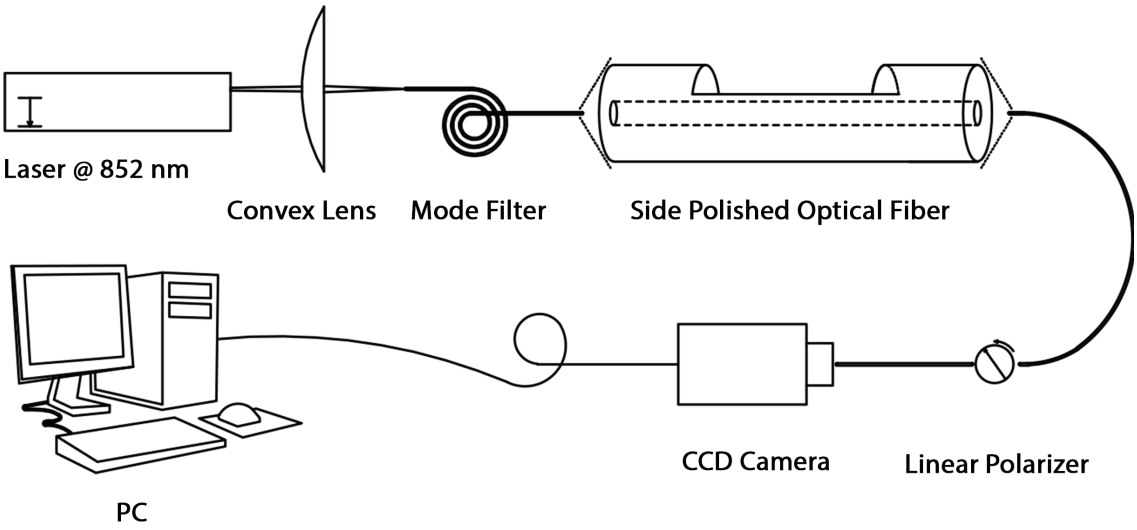

Figure 5.2. Schematic sketch of the single-mode experiment

LP_{11} mode.

After we reached single-mode propagation, initially the output of unpolished, i.e., output of standard optical fiber was checked with the linear polarizer. As expected the output light was linearly polarized. Then we set the setup with SPOF. The output measurements were taken for every 10° angle of the linear polarizer. These measurements were performed for three different angles of the input polarization, e.g, 0°, 45° and 90° according to laboratory axis.

CHAPTER 6

RESULTS AND DISCUSSION

6.1. Modal Field Simulations of the Guided Modes

In two-mode experiment there exist LP_{01} and LP_{11} modes together. At the output of this experiment we can measure the total power and the intensity distribution of the mode content. But it is not known which mode contributes what percentage to the total power. To find out percentage of the contributions, Maxwell Equations of the guided modes were simulated in MATLAB. Mode field simulations are performed for TM_{01}, TE_{01}, HE_{11} and HE_{21} modes. Their combinations generate linearly polarized LP modes (see Section 2.3).

The total mode content of the two-mode propagation basically depends on three factors. These are lobe orientation and polarization state of LP_{11} mode, polarization state of LP_{01} mode and their power contributions. There are sixteen possible mode content combination of horizontal and vertical polarized LP_{01} and LP_{11} modes. For equal power contributions of vertical polarized fundamental mode LP_{01}^{V} and the four forms of LP_{11} mode, the symbolic representations and the simulation results of eight possible combinations are illustrated in Figure 6.1. The symmetrical form of these distributions are valid for also horizontal polarized LP_{01}^{H} mode (see Figure 6.2).

In a combination, if the polarization states of the LP_{01} and LP_{11} modes are in the same direction, this causes a destructive effect in a half side of the resultant mode content, and constructive effect in the other half side. While the electric fields of the LP_{01} mode in the same direction with the electric fields of one lobe of LP_{11} mode, the other lobe is in the opposite direction. Besides, if the polarization states of the LP_{01} and LP_{11} modes are perpendicular to each other, this causes a constructive effect in the whole resultant mode content. This is due to vectorial addition of electric fields perpendicular to each other.

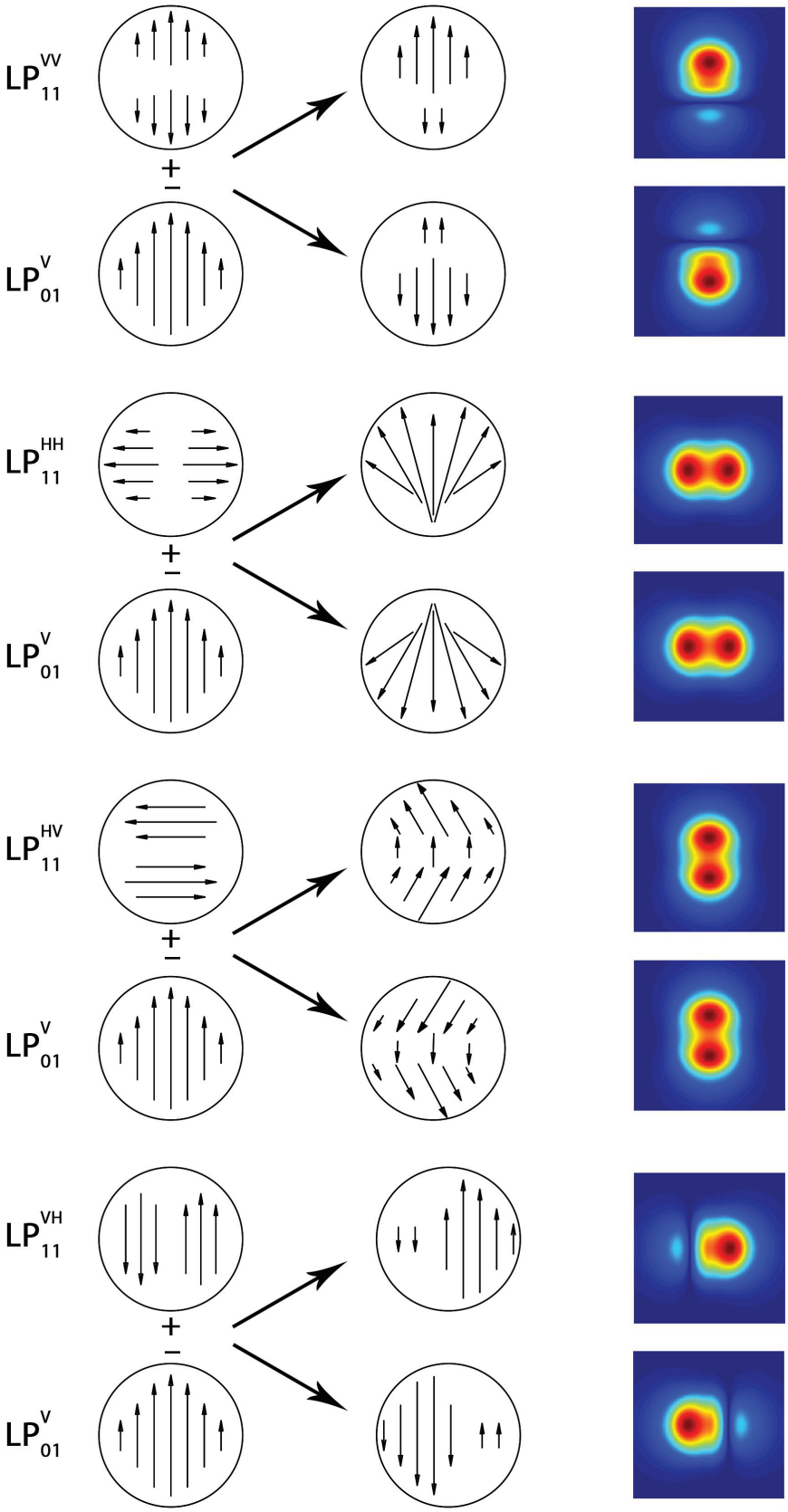

Figure 6.1. Possible combinations in terms of the symbolic electric field and simulated intensity distributions of LP_{01}^{V} and LP_{11} modes

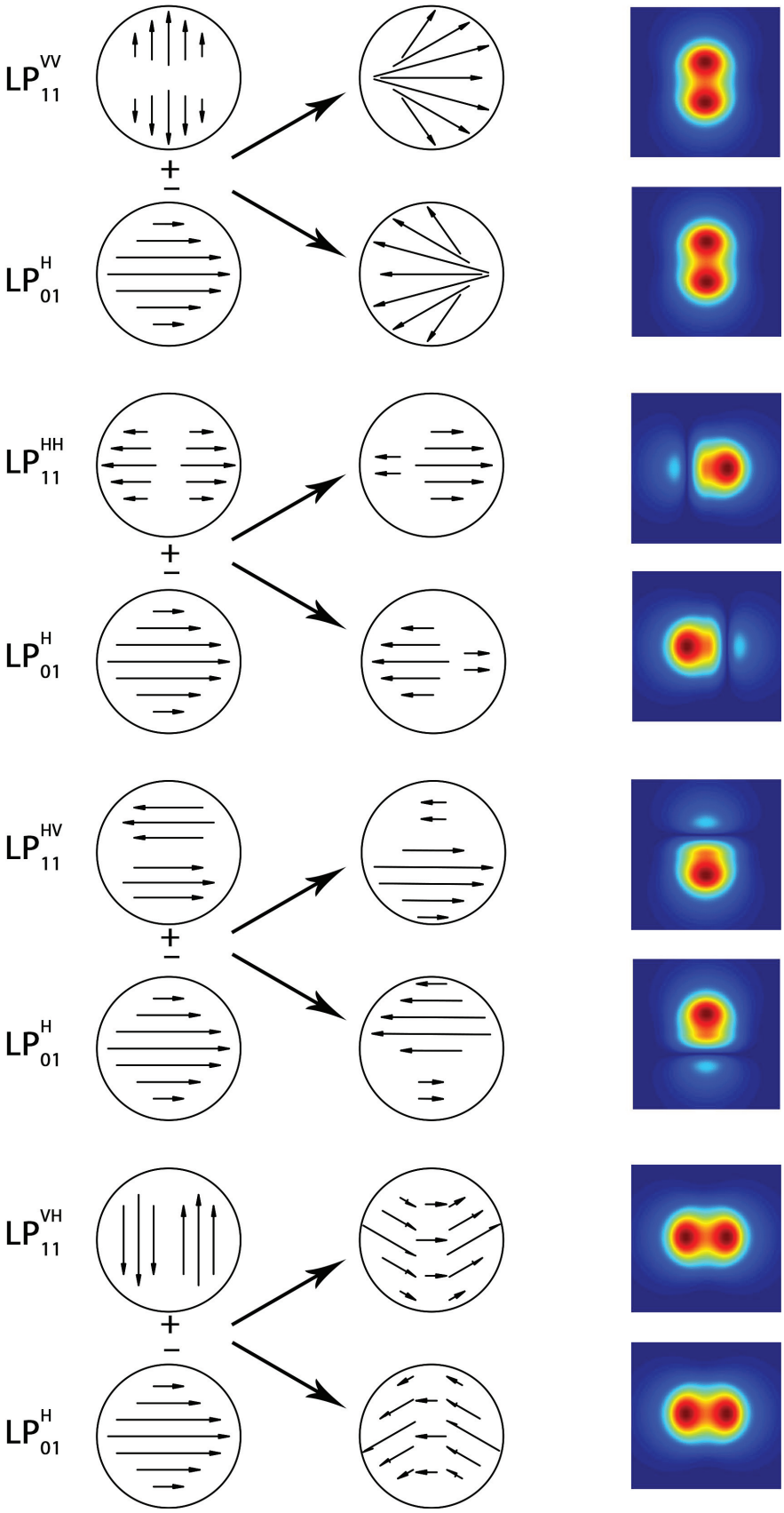

Figure 6.2. Possible combinations in terms of the symbolic electric field and simulated intensity distributions of LP_{01}^{H} and LP_{11} modes

6.2. Matching Experimental Data with MATLAB Simulations

In the two-mode experiment there are different mode combinations according to input polarization. Mode contents of the measurements are unknown. To figure out the contents, measurement results are matched with simulation results. The matching method is finding minimum error. Firstly size and orientation of the measurement result is fit on the simulation result. Then intensity difference, i.e., error is calculated via MATLAB. Simulated mode combination which provides minimum error determines the best-matched mode content.

In Figure 6.3, recorded images and the matched simulation results are illustrated. The shown CCD images belong to output of unpolished optical fiber and SPOF with respect to different angles of linear polarizer which are $0°$, $45°$ and $90°$. The calculated power percentages to the mode content of LP_{01} and LP_{11} modes are given in Table 6.1.

Table 6.1. Mode matching results of the two-mode experiment

Input Type	Percentage of LP_{01}	Percentage of LP_{11}
Unpolished optical fiber	%33	%67
SPOF with $0°$ linear polarizer	%25	%75
SPOF with $45°$ linear polarizer	%64	%36
SPOF with $90°$ linear polarizer	%41	%59

The result of unpolished optical fiber shows there are two LP modes exist, and they have only one polarization of direction, i.e., there doesn't exist any degenerate mode pair. Due to only one polarization direction existence in the fiber, the output intensity distribution of the mode content concentrates to one side of the output.

However, as seen in Figure 6.3 in the two-mode SPOF experiment, for three critical angles of the linear polarizer the power never be zeroized. Also, the percentages of the mode contributions are different for all measurements. This situation is the proof that at the side-polished area modes couple to each other. Hence, degenerate modes and phase shifts occur at the region 3. Since the output measurements were recorded via linear polarizer, their intensity distributions also concentrates to one side of the output.

Due to the mode coupling between LP modes and interaction between the electric field distributions of the LP_{01} and LP_{11} modes it is hard to characterize polarization

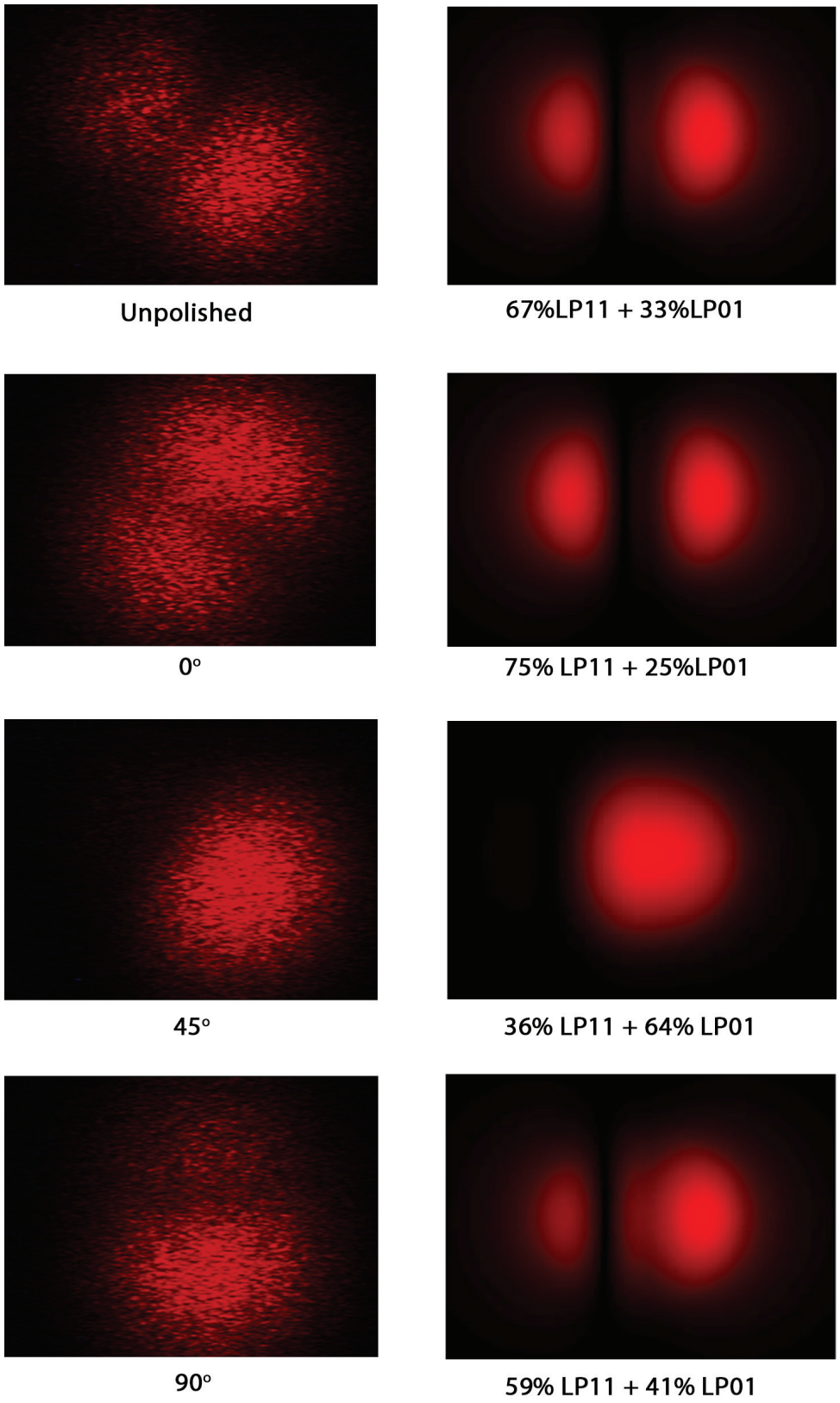

Figure 6.3. The recorded CCD Camera images of the two-mode propagation belong to unpolished optical fiber and the SPOF with respect to $0°$, $45°$ and $90°$ angles of the linear polarizer with matching simulation results

rotation and phase shift properties of the SPOF. To characterize the SPOF precisely, we need single-mode propagation.

6.3. Polarization and Phase Characterization of the Single-Mode Experiment

Measurement via CCD Camera provides us an image of the intensity distrubion of the optical fiber output. If we record images for every 10° angle of the linear polarizer, we reach relative power relation between the images. Since intensity of an electromagnetic wave P is proportional to the square of the electric field $\mathbf{E}^2$, we can also reach to electric field relation between the different angle of polarization. In the light of this information, normalized electic field amplitudes of the outputs listed in Table 6.2.

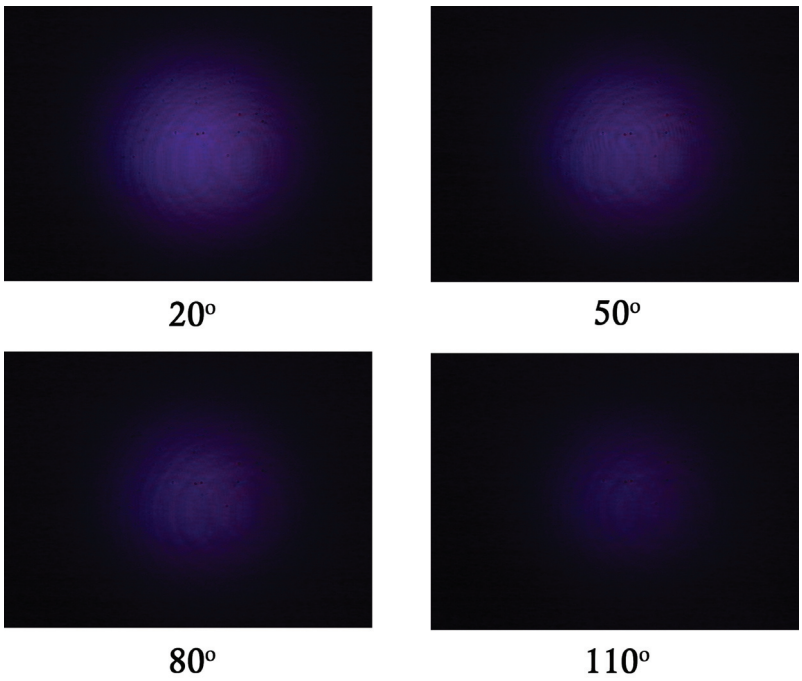

Figure 6.4. The samples of the recorded CCD Camera images of the single-mode propagation at the linear polarizer angles of 20°, 50°, 80°, 110°

Four images belong to the single-mode experiment with 90° polarization of input illustrated in Figure 6.4. The maximum intensity occurs at the 20° and the minimum occurs at 110° of the linear polarizer. Since light always exists in the interval of 90° of the linear polarizer, SPOF generate degenerate modes with phase shift. Considering phase shift between the degenerate LP_{01} modes, the state of polarization is no longer linear, but

Table 6.2. The normalized amplitude values of the electric fields according to the angles of the input polarization and the linear polarizer

Polarizer Angle	90° input polarization	45° input polarization	0° input polarization
0°	1.544	1.145	0.810
10°	1.585	1.272	0.856
20°	1.612	1.386	0.985
30°	1.583	1.484	1.091
40°	1.546	1.547	1.213
50°	1.469	1.565	1.324
60°	1.329	1.550	1.422
70°	1.240	1.481	1.469
80°	1.133	1.389	1.502
90°	1.034	1.268	1.469
100°	1.009	1.144	1.422
110°	0.969	1.086	1.324
120°	1.011	0.965	1.213
130°	1.035	0.835	1.091
140°	1.137	0.774	0.985
150°	1.238	0.831	0.856
160°	1.331	0.969	0.810
170°	1.470	1.082	0.662
180°	1.542	1.150	0.818
190°	1.582	1.273	0.857
200°	1.597	1.341	0.989
210°	1.590	1.487	1.098
220°	1.543	1.543	1.209
230°	1.467	1.559	1.321
240°	1.330	1.546	1.427
250°	1.241	1.480	1.465
260°	1.130	1.383	1.508
270°	1.031	1.267	1.463
280°	1.014	1.138	1.418
290°	0.972	1.091	1.329
300°	1.005	0.962	1.210
310°	1.038	0.830	1.096
320°	1.129	0.777	0.980
330°	1.128	0.838	0.852
340°	1.324	0.961	0.817
350°	1.465	1.088	0.658

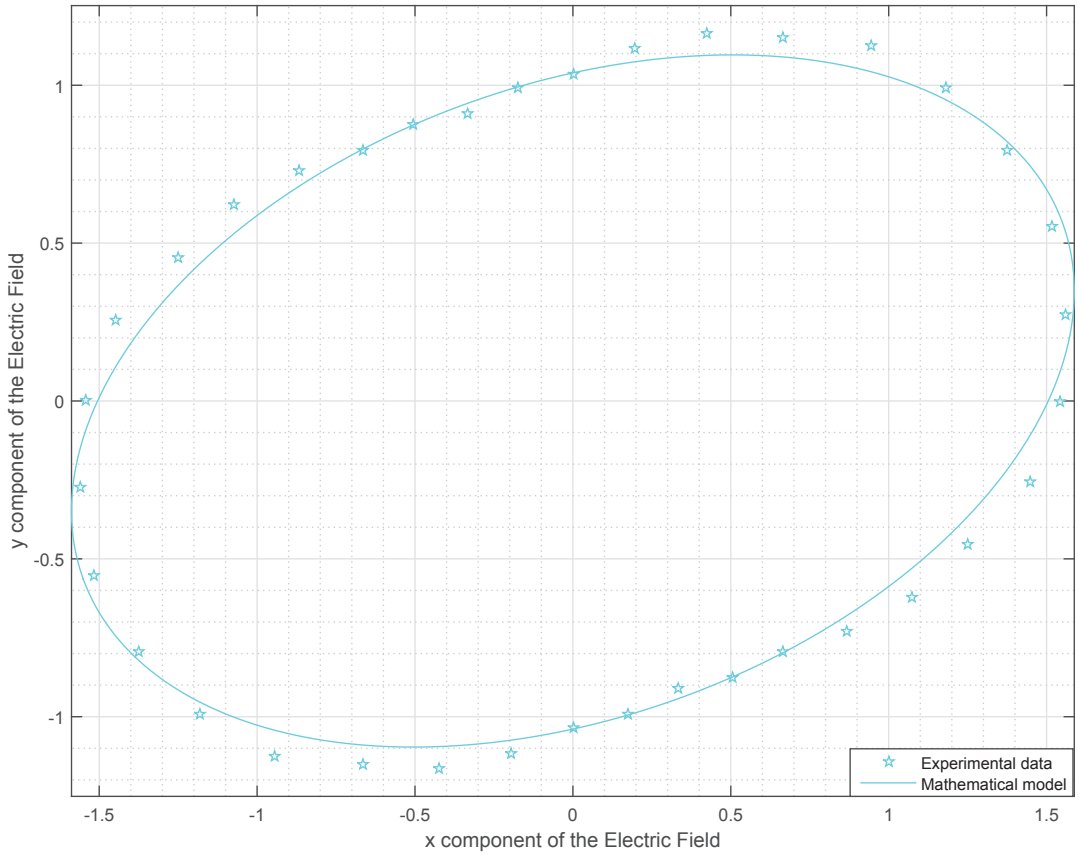

Figure 6.5. Experimental data and mathematical model of $90°$ input polarization angle

elliptical.

According to Table 6.2, electric field components, i.e., $\mathbf{E}_x$ and $\mathbf{E}_y$, were plotted. Since we obtain only intensity information from the CCD images, i.e., $\mathbf{E}^2$, vectorial information of the electric fields is exploited from the angle of the linear polarizer ζ. We can figure out the electric field components via

$$E_x\ \hat{\mathbf{x}} = \mathbf{E}\ cos(\zeta); \qquad E_y\ \hat{\mathbf{y}} = \mathbf{E}\ sin(\zeta). \tag{6.1}$$

Figure 6.5, 6.6 and 6.7 show the plotted experimental data and the mathematical models of elliptical polarization. There are three different ellipses according to angle of the input polarization, e.g., $90°$, $45°$ and $0°$. The experimental data wouldn't create perfect ellipses. This situation is caused by the noises which could occur because of CCD Camera, the linear polarizer and the ambient. While creating the mathematical model of polarization, we can eliminate the points which are distant from an elliptic scheme, i.e., errors. After we had canceled the error points, with the rest of the points the best-

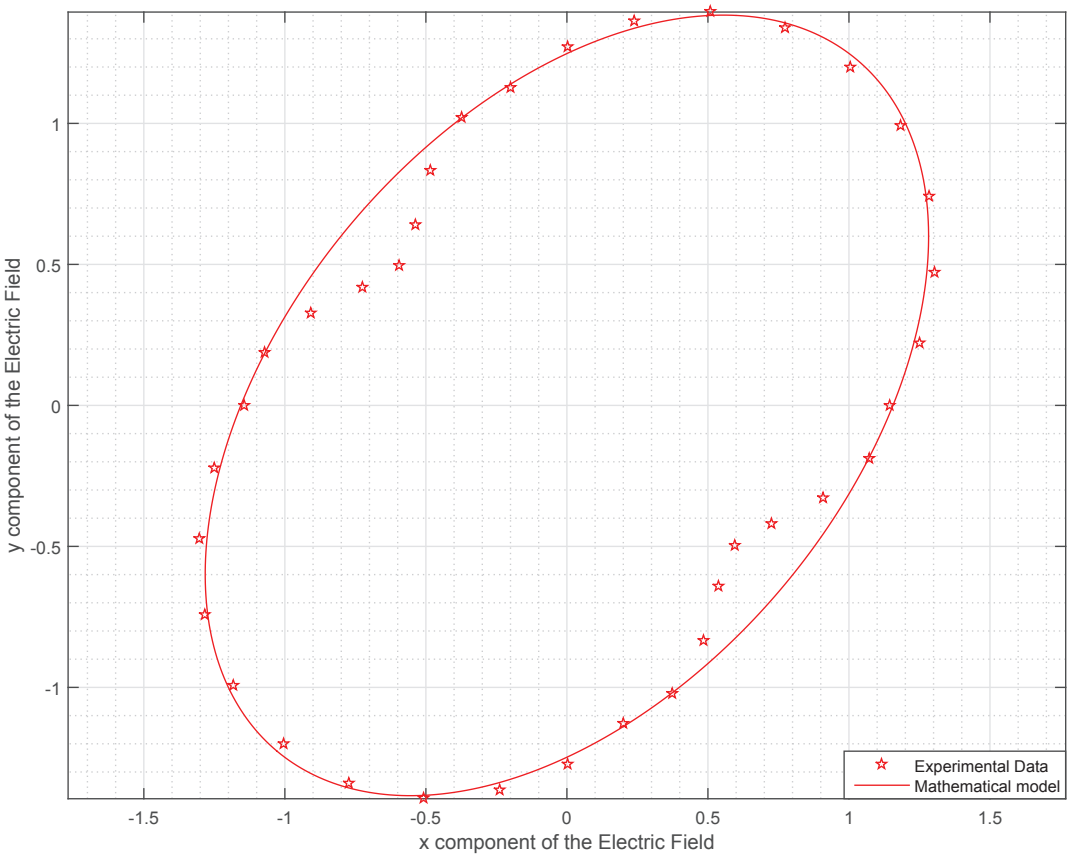

Figure 6.6. Experimental data and mathematical model of 45° input polarization angle

matched ellipses were generated. This process is done with least square method LSM via MATLAB.

From the mathematical model of ellipses (see Section 4.3) we calculated the phase difference between the degenerate LP_{01} modes, eccentricity and orientation of the ellipses that are listed in Table 6.3.

6.4. Overall Discussion

Studies were started with the two-mode experiment. The input polarization angle of the light source is known, but at the entrance of the side-polished area the angle between the polarization of the input light and the extraordinary axis is unknown. To investigate the effect of this unknown angle on the output and characterize the SPOF, the rotating linear polarizer was fitted between the output of the SPOF and the CCD Camera. Output images

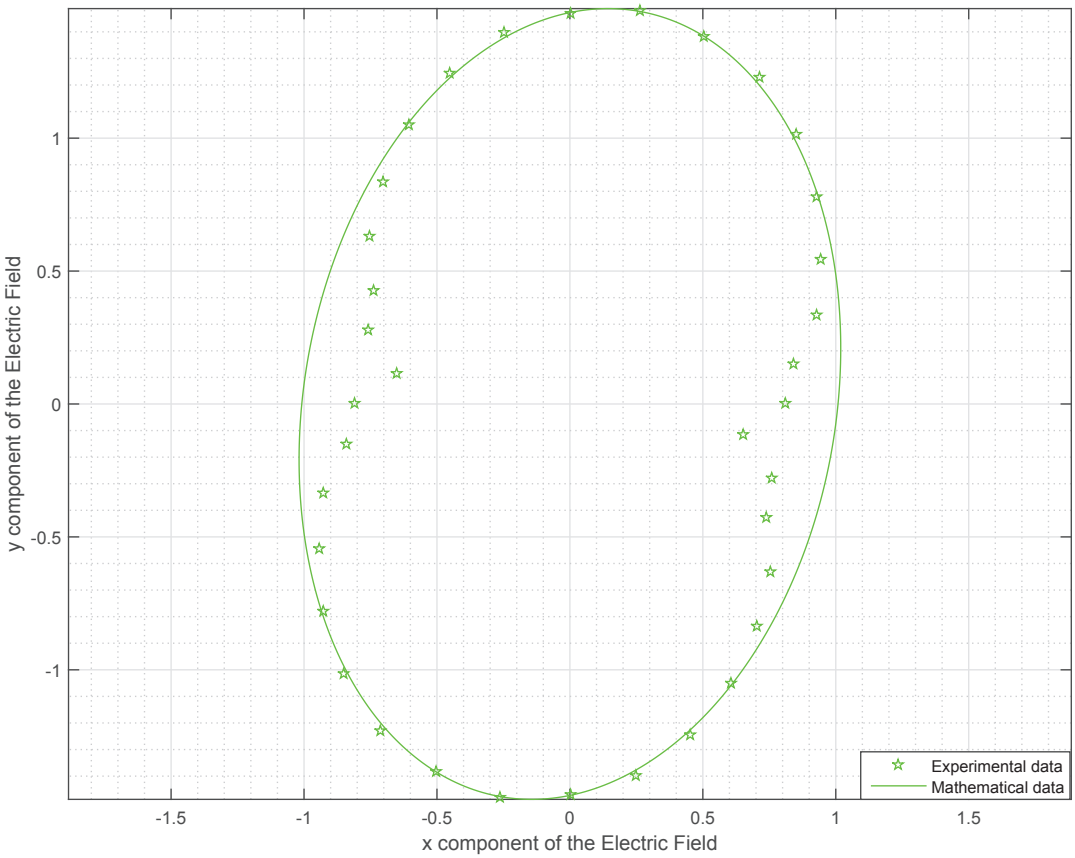

Figure 6.7. Experimental data and mathematical model of 0° input polarization angle

were recorded for different angles of the polarizer, and experiments were repeated for different angles of input polarization. The resultant images were evaluated with MATLAB and it shown there exist different mode contents for different angles of the polarizer. Also, existence of power at the output for different angles of the polarizer prove that output light is no longer linearly polarized. For all polarization angles of input, SOP of the output was always elliptical polarization, which means the SPOF is a birefringent device. Thus, it is deduced that at the side-polished area LP modes are coupled each other and quasi-degenerate modes occur with a phase delay. After light passes the side-polished area, degenerate LP modes propagate with different phases and for different SOP of the light there exist different mode contents. To analyze the resultant mode contents, recorded images were matched with computed modal intensity distributions using mode orthogonality. The best-matched results give us estimated mode contents, relative powers of LP modes to each other, mode orientations and information about SOP according to

the angle of the polarizer.

Table 6.3. Phase difference, eccentricity and orientations of the mathematically modeled ellipses

Polarization angle of input	Phase difference	Eccentricity	Orientation
$0°$	$82°$	0.7442	$80°$
$45°$	$80°$	0.7805	$51°$
$90°$	$72°$	0.7986	$19°$

Since mode coupling between LP_{01} and LP_{11} occurs in the two- mode experiment, phase shift characteristic of the SPOF couldn't be calculated accurately. Hence, to calculate phase shift, single-mode propagation was provided in the SPOF. In the single-mode experiment, at the side-polished area there occur quasi-degenerate modes. When the light is passing through the polished area, some percentage of the power radiates through the cladding- external environment interface. Due to the birefringent feature of the SPOF, at the polished area, occurred power losses and phase delays of the parallel and perpendicular polarized lights according to the extraordinary axis are different.

For each input polarization angle, the graphs were generated according to the power data obtained from the images recorded at $10°$ angle ranges of the polarizer in the single-mode experiment. Indeed, in theory, to draw an ellipse 3 points which are not linear are enough. However, because of the errors caused by impurities of the polarizer, ambient noise, etc., more data is needed to appear the ellipses. Thus, to draw each ellipses there are 36 data. The formed graphics with experimental data are not exact ellipse. To compute phase shift between degenerate modes, the data was mathematically modeled with using least-square method and the best matched ellipses were constructed (see Figures 6.5, 6.6 and 6.7). From the obtained ellipses, phase differences were computed and the other elliptic properties, i.e., eccentricity and orientation were also revealed (see Table 6.3). Therefore complete characterization of the side-polished optical fiber was accomplished.

Since the side polishing process is in micrometre level, it is very difficult that producing SPOFs having exactly the same geometry each time. Hence, depending on production-based nanometric impurities, the characteristic features of a SPOF would differ. Thus for every SPOF, characterization process should be repeated.

Moreover, optical properties of a side-polished optical fiber are sensitive to ambient refractive index. Observing the optical properties of the side-polished optical fiber,

i.e., state of polarization, phase shift etc. is widely used for designing optical fiber sensor. Therefore, our further detailed studies on the optical properties of the SPOF would be on improving sensing ambient refractive index and the other sensor application areas with this non-spectroscopic method.

CHAPTER 7

CONCLUSION

In this thesis, it is aimed to characterize polarization properties of side-polished optical fibers in details regarding attenuation and phase effects. Initially, the exact Maxwell modal solutions were computed with the parameters of the optical fiber used in the experiments. Intensity distributions of LP_{01}, LP_{11} and their combinations were obtained. The combinations can be tuned according to power contributions of LP modes, state of polarization and lobe orientation of LP_{11} mode. These LP mode intensity distributions were matched with the recorded images by the CCD Camera to expose the mode content of the optical fiber output in two-mode experiment. The best matched results gave us mode contents of the output. The mode contents of the output vary with the angle of the polarizer. Besides, for different SOP of the input mode contents differ. This situation shows that the side-polished region causes modes couple to each other in different ways depending on their SOP.

Next, the mode coupling was utilized to understand perturbation effect of the asymmetric geometry of side-polished optical fibers. In unpolished optical fiber, all modes are mutually orthogonal. However, in the side-polished area mode orthogonality are no longer valid. Due to the broken symmetry, the modes are coupling to each other and non-symmetrical modes occur. These non-symmetrical modes are affected in different ways depending on the angle Ω between SOP of the coming light and the ordinary axis a_o (which is flat side of the SPOF). The main effects of the SPOF on the input light are attenuation and phase shift. Since cladding is very thin at the side-polished area, attenuation is caused by virtue of power flow radiated through the cladding-outside interface. On the other hand, phase shift occurs because of the anisotropic structure of the SPOF, i.e., birefringence. The angle Ω specifies the mode coupling ratio between non-symmetrical modes and the phase shifts for both polarization states (parallel and perpendicular to extraordinary axis a_e). However, the angle Ω is an unknown parameter. Thus, to investigate its effect, the experiments were repeated for various orientation of input polarization.

According to the parameters of the experimental setups, a computational model was constructed. The parameters are input polarization orientation, the angle between polarization angle of the coming light to the beginning of the side-polished area and the ordinary axis, attenuation coefficients of the SPOF, phase shift coefficients of the SPOF

and the angle of the rotating linear polarizer. Since the side-polished region is a asymmetric medium, in this region mode coupling occurs between LP modes. Thus, to investigate the phase shift effect of the SPOF more precise, the single-mode experiment was held. In the single-mode experiment, 3 set of data were collected according to 3 different SOP of input. The output measurements were recorded in 10° intervals of the polarizer. When each set of data is gathered up in different graphs, a perfect ellipse does not occur because of the errors caused by the impurities of the polarizer, ambient noise, etc. Therefore, to eliminate errors these data were mathematically modeled with using the least square method and the best-matched ellipses were generated. There are 3 specific ellipses regarding SOP of input. The parameters of the ellipses which are phase difference, eccentricity, and orientation were disclosed computationally. The resultant phase differences between the degenerate LP_{01} modes are 82°, 80° and 72°, eccentricity of the ellipses are 0.7442, 0.7805 and 0.7986, orientation of the ellipses are 80°, 51° and 19° which corresponds to the angle of the input polarization 0°, 45° and 90° respectively. The fact that these three ellipses are quite different from each other regarding all parameters means that the SPOF has a nonlinear effect according to the angle of the input polarization orientation. And this effect leads to the phase shift and power loss of the incoming light in different amounts depending on the SOP of an input. To obtain these ellipses, 36 different intensity measurements were recorded for each experiments. Indeed, if a more accurate system is set up with decreased error level, a complete characterization of a SPOF can be achieved with a few measurements. This might be helpful for better optical sensor design.

The primary advantage of this method is that it is not spectroscopic. The spectroscopic ones are bulky and expensive. On the other hand, the non-spectroscopic methods, which measure output intensity of a SPOF, are not sophisticate and they are inexpensive systems. These systems are being used to sense the refractive index of the ambient. With our detailed study, we have provided a better understanding of phase and polarization properties. In addition, the loss between the non-symmetrical modes in the side-polished region has been taken into account. Therefore we expect it to contribute to the design of more sensitive optical sensors. Furthermore, we predict that this kind of structures have a potential to be used for a coherent communication device. The function of the device could be phase-polarization modulator or mode converter. Modulation of phase and polarization could be achieved by the birefringent property which can be altered by the refractive index of the SPOF. And a mode converter could be realized with the mode coupling feature of the side-polished optical fiber.

REFERENCES

[1] Sharma, A. K.; Jha, R.; Gupta, B. D. Fiber-Optic Sensors Based on Surface Plasmon Resonance: A Comprehensive Review. *IEEE Sensors Journal*. 2007. https://doi.org/10.1109/JSEN.2007.897946.

[2] Homola, J. Optical Fiber Sensor Based on Surface Plasmon Excitation. *Sensors Actuators B. Chem.* **1995**. https://doi.org/10.1016/0925-4005(95)01714-3.

[3] Ramakrishnan, M.; Rajan, G.; Semenova, Y.; Farrell, G. Overview of Fiber Optic Sensor Technologies for Strain/Temperature Sensing Applications in Composite Materials. *Sensors (Switzerland)*. 2016. https://doi.org/10.3390/s16010099.

[4] Agrell, E.; Karlsson, M.; Chraplyvy, A. R.; Richardson, D. J.; Krummrich, P. M.; Winzer, P.; Roberts, K.; Fischer, J. K.; Savory, S. J.; Eggleton, B. J.; et al. Roadmap of Optical Communications. *J. Opt. (United Kingdom)* **2016**. https://doi.org/10.1088/2040-8978/18/6/063002.

[5] Kim, K. T.; Kim, H. K.; Hwangbo, S.; Choi, S.; Lee, B. H.; Oh, K. Characterization of Evanescent Wave Coupling in Side-Polished Hollow Optical Fiber and Its Application as a Broadband Coupler. *Opt. Commun.* **2005**. https://doi.org/10.1016/j.optcom.2004.10.008.

[6] Álvarez-Herrero, A.; Guerrero, H.; Belenguer, T.; Levy, D. High-Sensitivity Temperature Sensor Based on Overlay on Side-Polished Fibers. *IEEE Photonics Technol. Lett.* **2000**. https://doi.org/10.1109/68.868002.

[7] Takeo, T.; Hattori, H. Optical Fiber Sensor for Measuring Refractive Index. *Jpn. J. Appl. Phys.* **1982**. https://doi.org/10.1143/JJAP.21.1509.

[8] Villuendas, F.; Pelayo, J. Optical Fibre Device for Chemical Seming Based on Surface Plasmon Excitridon. *Sensors Actuators A. Phys.* **1990**. https://doi.org/10.1016/0924-4247(90)87104-Q.

[9] Nguyen, T. T.; Lee, E.-C.; Ju, H. Bimetal Coated Optical Fiber Sensors Based on Surface Plasmon Resonance Induced Change in Birefringence and Intensity.

Opt. Express **2014**. https://doi.org/10.1364/OE.22.005590.

[10] Alan Snyder, L. *Waveguide Theory*; 1983. https://doi.org/10.1007/978-1-4613-2813-1.

[11] Leung, A.; Shankar, P. M.; Mutharasan, R. A Review of Fiber-Optic Biosensors. *Sensors and Actuators, B: Chemical*. 2007. https://doi.org/10.1016/j.snb.2007.03.010.

[12] Mescia, L.; Prudenzano, F. Advances on Optical Fiber Sensors. *Fibers* **2013**. https://doi.org/10.3390/fib2010001.

[13] Messica, A.; Greenstein, A.; Katzir, A. Theory of Fiber-Optic, Evanescent-Wave Spectroscopy and Sensors. *Appl. Opt.* **1996**. https://doi.org/10.1364/AO.35.002274.

[14] Milosevic, M. On the Nature of the Evanescent Wave. *Appl. Spectrosc.* **2013**. https://doi.org/10.1366/12-06707.

[15] Giallorenzi, T. G.; Bucaro, J. A.; Dandridge, A.; Sigel, G. H.; Cole, J. H.; Rashleigh, S. C.; Priest, R. G. Optical Fiber Sensor Technology. *IEEE Trans. Microw. Theory Tech.* **1982**. https://doi.org/10.1109/TMTT.1982.1131089.

[16] Lee, B. Review of the Present Status of Optical Fiber Sensors. *Optical Fiber Technology*. 2003. https://doi.org/10.1016/S1068-5200(02)00527-8.

[17] Zhao, J.; Cao, S.; Liao, C.; Wang, Y.; Wang, G.; Xu, X.; Fu, C.; Xu, G.; Lian, J.; Wang, Y. Surface Plasmon Resonance Refractive Sensor Based on Silver-Coated Side-Polished Fiber. *Sensors Actuators, B Chem.* **2016**. https://doi.org/10.1016/j.snb.2016.02.020.

[18] Lin, H.-Y.; Tsai, W.-H.; Tsao, Y.-C.; Sheu, B.-C. Side-Polished Multimode Fiber Biosensor Based on Surface Plasmon Resonance with Halogen Light. *Appl. Opt.* **2007**. https://doi.org/10.1364/AO.46.000800.

[19] Grattan, K. T. V.; Sun, T. Fiber Optic Sensor Technology: An Overview. *Sensors Actuators, A Phys.* **2000**. https://doi.org/10.1016/S0924-4247(99)00368-4.

[20] Gaston, A.; Pérez, F.; Sevilla, J. Optical Fiber Relative-Humidity Sensor with Polyvinyl Alcohol Film. *Appl. Opt.* **2004**. https://doi.org/10.1364/AO.43.004127.

[21] Hayashi, K. Optical Chemical Sensor. *IEEJ Trans. Sensors Micromachines* **2015**. https://doi.org/10.1021/cr068102g.

[22] Personick, S. D. Fundamentals of Optical Fiber Communications. *Fundam. Opt. Fiber Commun.* **1981**. https://doi.org/10.1016/B978-0-12-079151-4.50010-8.

[23] Tripathi, S. M.; Kumar, A.; Marin, E.; Meunier, J. P. Side-Polished Optical Fiber Grating-Based Refractive Index Sensors Utilizing the Pure Surface Plasmon Polariton. *J. Light. Technol.* **2008**. https://doi.org/10.1109/JLT.2007.913585.

[24] Bilro, L.; Alberto, N. J.; Sá, L. M.; De Lemos Pinto, J.; Nogueira, R. Analytical Analysis of Side-Polished Plastic Optical Fiber as Curvature and Refractive Index Sensor. *J. Light. Technol.* **2011**. https://doi.org/10.1109/JLT.2011.2105462.

[25] Jang, H. S.; Park, K. N.; Kang, C. D.; Kim, J. P.; Sim, S. J.; Lee, K. S. Optical Fiber SPR Biosensor with Sandwich Assay for the Detection of Prostate Specific Antigen. *Opt. Commun.* **2009**. https://doi.org/10.1016/j.optcom.2009.03.078.

[26] Khalaf, A. L.; Mohamad, F. S.; Rahman, N. A.; Lim, H. N.; Paiman, S.; Yusof, N. A.; Mahdi, M. A.; Yaacob, M. H. Room Temperature Ammonia Sensor Using Side-Polished Optical Fiber Coated with Graphene/Polyaniline Nanocomposite. *Opt. Mater. Express* **2017**. https://doi.org/10.1364/OME.7.001858.

[27] Sun, H.; Pyajt, A.; Luo, J.; Shi, Z.; Hau, S.; Jen, A. K. Y.; Dalton, L. R.; Chen, A. All-Dielectric Electrooptic Sensor Based on a Polymer Microresonator Coupled Side-Polished Optical Fiber. *IEEE Sens. J.* **2007**. https://doi.org/10.1109/JSEN.2006.886901.

[28] Agrawal, G. P. *Applications of Nonlinear Fiber Optics*; 2008. https://doi.org/10.1016/B978-0-12-374302-2.X5001-3.

[29] Meléndez, J.; Carr, R.; Bartholomew, D.; Taneja, H.; Yee, S.; Jung, C.; Furlong, C.

Development of a Surface Plasmon Resonance Sensor for Commercial Applications. *Sensors Actuators, B Chem.* **1997**. https://doi.org/10.1016/S0925-4005(97)80237-7.

[30] Agrawal, G. P. Polarization Effects. In *Nonlinear Fiber Optics*; 2013. https://doi.org/10.1016/B978-0-12-397023-7.00006-1.

[31] Hyle Park, B.; Pierce, M. C.; Cense, B.; de Boer, J. F. Jones Matrix Analysis for a Polarization-Sensitive Optical Coherence Tomography System Using Fiber-Optic Components. *Opt. Lett.* **2004**. https://doi.org/10.1364/OL.29.002512.

[32] Gafsi, R.; El-Sherif, M. A. Analysis of Induced-Birefringence Effects on Fiber Bragg Gratings. *Opt. Fiber Technol.* **2000**. https://doi.org/10.1006/ofte.2000.0333.

[33] Kaminow, I. P. Papers Polarization in Optical Fibers. *IEEE J. Quantum Electron.* **1981**. https://doi.org/10.2307/1125631.

[34] Ulrich, R.; Rashleigh, S. C.; Eickhoff, W. Bending-Induced Birefringence in Single-Mode Fibers. *Opt. Lett.* **1980**. https://doi.org/10.1364/OL.5.000273.

[35] Gloge, D. Weakly Guiding Fibers. *Appl. Opt.* **1971**. https://doi.org/10.1364/AO.10.002252.

[36] Snyder, A. W. Weakly Guiding Optical Fibers. *J. Opt. Soc. Am.* **1980**. https://doi.org/10.1364/JOSA.70.000405.

[37] Marcuse, D. *Theory of Dielectric Optical Waveguides*; 1974. https://doi.org/10.1016/B978-0-12-470951-5.50011-1.

[38] Marcuse, D.; Ladouceur, F.; Love, J. D. Vector Modes of D-Shaped Fibres. *IEE Proc. J Optoelectron.* **1992**. https://doi.org/10.1049/ip-j.1992.0021.

[39] Huang, W.-P. Coupled-Mode Theory for Optical Waveguides: An Overview. *J. Opt. Soc. Am. A* **1994**. https://doi.org/10.1364/JOSAA.11.000963.

[40] Yariv, A. Coupled-Mode Theory for Guided-Wave Optics. *IEEE J. Quantum Electron.* **1973**. https://doi.org/10.1109/JQE.1973.1077767.

[41] Denman, E. D. Coupled Mode Theory. *J. Math. Anal. Appl.* **1968**. https://doi.org/10.1016/0022-247X(68)90210-2.

[42] Born, M.; Wolf, E.; Hecht, E. *Principles of Optics: Electromagnetic Theory of Propagation, Interference and Diffraction of Light. Phys. Today* **2000**. https://doi.org/10.1063/1.1325200.

[43] Luo, H.; Sun, Q.; Li, Y.; Liu, D.; Zhang, L. Highly Birefringent D-Shaped Microfiber and Its Application in High-Sensitive Optical Sensing. *IEEE Sens. J.* **2016**. https://doi.org/10.1109/JSEN.2016.2524624.

[44] Spadoti, Spadoti, D. H.; Borges, B. H. V.; Romero, M. A. Birefringence Enhancement by Using D-Shaped Microstructured Optical Fibers. *J. Opt. A Pure Appl. Opt.* **2009**. https://doi.org/10.1088/1464-4258/11/8/085105.

[45] Kogelnik, H.; Winzer, P. J. Modal Birefringence in Weakly Guiding Fibers. *J. Light. Technol.* **2012**. https://doi.org/10.1109/JLT.2012.2193872.

[46] Corning HI 1060 & RC HI 1060 Specialty Optical Fibers. https://www.corning.com/media/worldwide/csm/documents/HI 1060 Specialty Fiber PDF.pdf